

DETECTION OF DEPENDENCE PATTERNS WITH DELAY

Julien Chevallier*, Thomas Laloë

Univ. Nice Sophia Antipolis, CNRS, LJAD, UMR 7351, 06100 Nice, France.

Abstract

The Unitary Events (UE) method is a popular and efficient method used this last decade to detect dependence patterns of joint spike activity among simultaneously recorded neurons. The first introduced method is based on binned coincidence count ([Grün, 1996](#)) and can be applied on two or more simultaneously recorded neurons. Among the improvements of the methods, a transposition to the continuous framework has recently been proposed in ([Muñoz and Borgelt, 2014](#)) and fully investigated in ([Tuleau-Malot et al., 2014](#)) for two neurons. The goal of the present paper is to extend this study to more than two neurons. The main result is the determination of the limit distribution of the coincidence count. This leads to the construction of an independence test between $L \geq 2$ neurons. Finally we propose a multiple test procedure via a Benjamini and Hochberg approach ([Benjamini and Hochberg, 1995](#)). All the theoretical results are illustrated by a simulation study, and compared to the UE method proposed in ([Grün et al., 2002](#)). Furthermore our method is applied on real data.

Mathematical Subject Classification. 62M07, 62F03, 62H15, 62P10.

Keywords. Unitary Events, Coincidence pattern, Neuronal assemblies, Independence tests, Poisson processes.

Contents

1	Introduction	2
2	Notions of coincidence and the classical UE methods	3
3	Study of the delayed coincidence count	5
4	Illustration Study: Poissonian Framework	9
5	Illustration Study: Non-Poissonian framework	12
6	Illustration on real data	16
7	Conclusion	17
8	Proofs	19

*Corresponding author: e-mail: julien.chevallier@unice.fr

1 Introduction

The communication between neurons relies on their capacity to generate characteristic electric pulses called action potentials. These action potentials are usually assumed to be identical stereotyped events. Their time of occurrence (called spike) is considered as the relevant information. That is why the study of spike frequencies (firing rates) of neurons plays a key role in the comprehension of the information transmission in the brain (Abeles, 1982; Gerstein and Perkel, 1969; Shinomoto, 2010). Such neuronal signals are recorded from awake behaving animals by insertion of electrodes into the cortex to record the extracellular signals. Potential spike events are extracted from these signals by threshold detection and, by spike sorting algorithms, sorted into the spike signals of the individual single neurons. After this preprocessing, we dispose of sequences of spikes (called spike trains).

The analysis of spike trains has been an area of very active research for many years (Brown et al., 2004). Although the rules underlying the information processing in the brain are still under burning debate, the detection of correlated firing between neurons is the objective of many studies in the recent years (Roy et al., 2007; Dong et al., 2008; Pillow et al., 2008). This synchronization phenomenon may take an important role in the recognition of sensory stimulus. In this article, the issue of detecting dependence patterns between simultaneously recorded spike trains is addressed. Despite the fact that some studies used to consider neurons as independent entities (Barlow, 1972), many theoretical works consider the possibility that neurons can coordinate their activities (Hebb, 1949; Palm, 1990; Sakurai, 1999; von der Malsburg, 1981). The understanding of this synchronization phenomenon (Singer, 1993) required the development of specific descriptive analysis methods of spike-timing over the last decades: cross-correlogram (Perkel et al., 1967), gravitational clustering (Gerstein et al., 1985) or joint peristimulus time histogram (JPSTH, (Aertsen et al., 1989)). Following the idea that the influence of a neuron over others (whether exciting or inhibiting) results in the presence (or absence) of coincidence patterns, Grün and collaborators developed one of the most popular and efficient method used this last decade: the Unitary Events (UE) analysis method (Grün, 1996) and the corresponding independence test, which detects where dependence lies by assessing p-values (A Unitary Event is a spike synchrony that recurs more often than expected by chance). This method is based on a binned coincidence count that is unfortunately known to suffer a loss in synchrony detection, but this flaw has been corrected by the multiple shift coincidence count (Grün et al., 1999).

In order to deal with continuous time processes, a new method (Multiple Tests based on a Gaussian Approximation of the Unitary Events method), based on a generalization of this count, the delayed coincidence count, has recently been proposed for two parallel neurons (Section 3.1 of (Tuleau-Malot et al., 2014)). The results presented in this article are in the lineage of this newest method and are applied on continuous point processes (random set of points which are modelling spike trains). Testing independence between real valued random variables is a well known problem, and various techniques have been developed, from the classical chi-square test to re-sampling methods for example. The interested reader may look at (Lehmann and Romano, 2005). Some of these methods and more general surrogate data methods have been applied on binned coincidence count, since the binned process transforms the spike train in vectors of finite dimension. However, the case of point processes that are not preprocessed needs other tools and remains to study. Although the binned method can deal with several neurons (six simultaneously recorded neurons are analysed in (Grün et al., 2002), both of the improvements (Multiple Shift and MTGAUE) can only consider pairs of neurons. Thus, our goal is to generalize the method introduced in (Tuleau-Malot et al., 2014) for more than two neurons. Unlike MTGAUE, our test is not designed to be performed on multiple time windows. However it can be multiple with respect to the different possible patterns composed from $n \geq 2$ neurons (see Section 5.3).

In Section 2, we introduce the different notions of coincidence used through this article. In Section 3, a test is established and the asymptotic control of its false positive rate is proven. In Section 4 our test is confronted to the original UE method on simulated data and the accuracy of the Gaussian approximation is verified. In Section 5 the relevance of our method when our main theoretical assumptions are weakened is also empirically put on test. Section 6 presents an illustration on real data. All the technical proofs are given in the Appendix.

2 Notions of coincidence and the classical UE methods

In order to detect synchronizations between the involved neurons, different notions of coincidence can be considered. Informally, there is a coincidence between neurons when they each emit a spike more or less simultaneously. This notion has already been used in UE methods (Grün et al., 2002) and is based on the following idea: a real dependency between $n \geq 2$ neurons should be characterized by an unusually large (or low) number of coincidence (Grammont and Riehle, 2003; Grün, 1996; Tuleau-Malot et al., 2014).

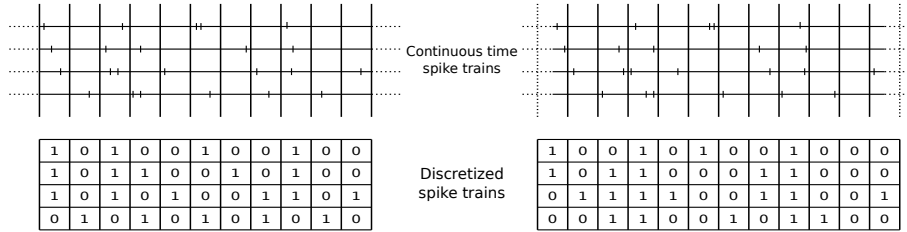
2.1 Two notions of coincidence

The UE method (see (Grün, 1996)) considers discretized spike trains at a resolution ℓ of typically 1 or 0.1 millisecond. Therefore, in the discrete-time framework, each trial consists of a set of n spike trains (one for each recorded neuron), each spike train being represented by a sequence of 0 and 1 of length S . Since it is quite unlikely that two spikes occur at exactly the same time at this resolution ℓ , spike trains are binned and clipped at a coarser level. More precisely for a fixed bin size $\Delta = d\ell$ (d being an integer), a new sequence of length S/d of 0 and 1 is associated to each spike train (1 if at least one spike occurs in the corresponding bin, 0 otherwise). For more precise informations on the binning procedure and the link with point processes we refer the interested reader to (Tuleau-Malot et al., 2014).

A : Simultaneously recorded neurons

Bin	1	2	3	...	(S/d)-1	S/d
Neuron 1	1	1	0	...	0	1
Neuron 2	0	1	0	...	1	1
Neuron 3	0	1	0	...	0	1
Neuron 4	0	0	1	...	1	1
\mathcal{L}_w	{1}	{1, 2, 3}	{4}	...	{2, 4}	{1, 2, 3, 4}

B : Discretization of spike trains



C : Delayed coincidence count

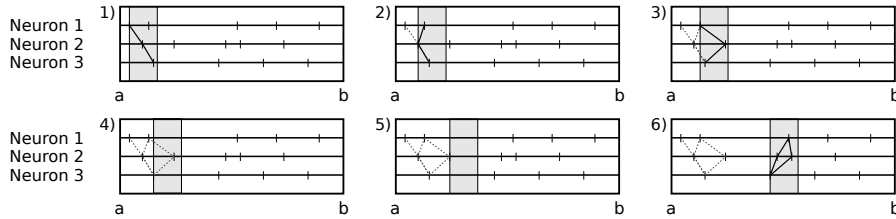


Figure 1: In **A**, 4 parallel binary processes of length S are displayed. At each time step, the constellation and its corresponding subset of $\{1, 2, 3, 4\}$ are given. For instance, the constellation associated to the first bins is the vector $(1, 0, 0, 0)$ and the corresponding subset is $\{1\}$. In **B**, illustration of the UE method with two different choices of bins of the same size (the results are different, for example the constellation full of 1s is present in the second case and not in the first one). In **C**, an illustration of the six first steps in the dynamical computation of the delayed coincidence count. Here, there are 3 parallel time point processes. We consider the full pattern, i.e. $\mathcal{L} = \{1, 2, 3\}$. The grey rectangle represents the sliding time window of length δ . The bold lines denote the coincidence patterns counted at each step and the grey dashed ones denote the coincidence pattern which have been counted in one the previous steps. At each of steps 1, 2 and 3, exactly one coincidence is counted. At steps 4 and 5, no coincidence is detected. And, at step 6, two coincidences are counted.

A constellation or pattern is a vector of size n of 0 and 1 (see Figure 1 or (Grün et al., 2002)). Of course, there are 2^n different constellations. The UE statistic associated to some constellation w consists in counting the number of occurrences of such w in the set of S/d vectors of size n .

However, as shown in Figure 1, this method largely depends on the bin choice and it has been proven in (Grün et al., 1999) that this can lead in the case $n = 2$ to up to 60% of loss in detection when Δ is of the order of the range of interaction.

Then, we focus on another coincidence count that deals with continuous data. This notion of delayed coincidence count is pretty natural and was used in (Muñoz and Borgelt, 2014) or (Borgelt and Muñoz, 2013) in a simplified formalism. For sake of simplicity, we use the same formalism of point processes as in (Tuleau-Malot et al., 2014). Nevertheless, we give the correspondences, whenever it is possible, between their formalism and ours (see Table 1).

Considering N_1, \dots, N_n , some point processes on $[a, b]$, and $\mathcal{L} \subset \{1, \dots, n\}$ a set of indices of cardinal $L \geq 2$, the *delayed coincidence count* $X_{\mathcal{L}}$ (of delay $\delta < (b - a)/2$) over the neurons of subset \mathcal{L} in the time window $[a, b]$ is given by

$$X_{\mathcal{L}} = X_{\mathcal{L}}(\delta) = \sum_{(x_1, \dots, x_L) \in \prod_{l \in \mathcal{L}} N_l} \mathbf{1}_{\left| \max_{i \in \{1, \dots, L\}} x_i - \min_{i \in \{1, \dots, L\}} x_i \right| \leq \delta}. \quad (1)$$

The delayed coincidence count can be explained in the following way (see Figure 1):

- Fix some duration parameter δ which is the equivalent of the bin size Δ ,
- Count how many times each neuron in \mathcal{L} spikes almost at the same time, modulo the delay δ .

	(Muñoz and Borgelt, 2014)	(Borgelt and Muñoz, 2013)	This article
Time window	$[0, T]$	Not relevant	$[a, b]$
Subset	A	A	\mathcal{L}
Delay	r	w	δ
Number of coincidences	Not relevant	$ \mathcal{E}(A, w) $ (page 3)	$X_{\mathcal{L}}$
Spike-train synchrony	$Supp_{ A }(E^A)$	$ \mathcal{E}(A, w) $ (page 4)	Not relevant

Table 1: List of the correspondences in the notations between three papers: (Muñoz and Borgelt, 2014), (Borgelt and Muñoz, 2013) and this article.

Remark 2.1. For computational reasons, Muñoz and Borgelt compute some non-overlapping coincidence count, which corresponds to the last line of the Table 1. They impose the condition that at most one coincidence per spike is counted. The statistical study of this non-overlapping coincidence count is not the scope of this article. Although interesting, this is a much more challenging question.

2.2 Original UE method

The notion of constellation is closely linked to the binning procedure and is not relevant in the continuous time framework. In this work, we fix some subset of neurons, denoted \mathcal{L} , and count how many times the neurons of \mathcal{L} admit nearly simultaneous activity. However, there is a canonical correspondence between constellations and set of indices (see Figure 1). Then, in order to harmonize the notations between both methods, let us denote $\mathcal{L}(w)$ the set of indices corresponding to the constellation w .

To detect dependency between neurons, two estimators of the expected coincidence count are compared. The first one is the empirical mean \bar{m}_w of the number of occurrences of a given constellation w through M trials,

$$\bar{m}_w = \frac{1}{M} \sum_{k=1}^M m_w^{(k)},$$

where $m_w^{(k)}$ is the number of occurrences of w during the k^{th} trial. This estimator is consistent (that is, converges towards the expected value of the number of occurrences) even with dependency between the spike trains. The second one is consistent only under the independence hypothesis, and is given by

$$\hat{m}_{g,w} = \frac{S}{d} \prod_{l \in \mathcal{L}(w)} \hat{p}_l \prod_{k \notin \mathcal{L}(w)} (1 - \hat{p}_k), \quad (2)$$

where \hat{p}_i is the empirical probability of finding a spike in a bin of neuron i .

This enables the construction of the test described in (Grün et al., 2002) and based on the comparison between the statistic $M\bar{m}_w$ and a quantile of the Poisson distribution $\mathcal{P}(M\hat{m}_{g,w})$ where M is the number of trials. Most of the time only tests by upper values are computed (Grün, 1996; Grün et al., 2002). However, following the study of (Tuleau-Malot et al., 2014), we have decided to focus on symmetric tests. Hence, the symmetric test based on the UE method rejects the independence hypothesis when \bar{m}_w is too different from $\hat{m}_{g,w}$. However, such a test necessarily makes mistakes. For example, a *false positive* corresponds to an incorrect rejection of the null hypothesis. Hence, an a priori upper bound on the false positive rate, that is the *significance level* (or just *level*), must be given in order to construct a decision rule. The symmetric independence test with level α based on the UE method is governed by the following rule: if

$$M\bar{m}_w \geq q_{1-\alpha/2} \quad \text{or} \quad M\bar{m}_w \leq q_{\alpha/2},$$

where q_x is the x -quantile of the Poisson distribution $\mathcal{P}(M\hat{m}_{g,w})$, then the independence hypothesis is rejected.

The UE method is applied under the hypothesis that the discrete processes modelling the spike trains of neurons are Bernoulli processes. The equivalent in the "continuous" framework is the Poisson process (as it can be seen in (Tuleau-Malot et al., 2014)). This leads to a different estimator of the expected coincidence count and a different test which are defined properly in the next section.

3 Study of the delayed coincidence count

Once the notion of coincidence is defined with respect to continuous data (Equation (1)), mathematical tools can be used to construct the desired independence test. The procedure is to provide the expected value and variance of the variable $X_{\mathcal{L}}$ in function of the firing rates. These computations classically imply a Gaussian approximation with respect to i.i.d trials. Unfortunately the firing rates are usually unknown. Thus the final step is to replace the firing rates by their estimator to compute the estimated expected value and variance. This plug-in procedure is known to change the underlying distribution. As in (Tuleau-Malot et al., 2014), the delta method provides the exact nature of this change.

In the continuous framework, a sample is composed of M observations of N_1, \dots, N_n which are the point processes associated to the spike trains of n neurons on a window $[a, b]$. The goal is to answer the following question:

Given \mathcal{L} a subset of $\{1, \dots, n\}$, are the processes N_l , $l \in \mathcal{L}$ independent?

To do this, a statistical test comparing the two hypotheses

$$\begin{cases} (\mathcal{H}_0) & \text{The processes } N_l, l \in \mathcal{L} \text{ are independent;} \\ (\mathcal{H}_1) & \text{The processes } N_l, l \in \mathcal{L} \text{ are not independent;} \end{cases}$$

is proposed.

In this section our test and its asymptotic relevance are introduced. First, let us present and discuss our main assumptions which are the same as in (Tuleau-Malot et al., 2014).

Assumption A1. N_1, \dots, N_n are Poisson processes.

This assumption can be resumed to an assumption of independence of a point process with respect to itself over the time, as Bernoulli processes in discrete settings.

Assumption A2. The Poisson processes N_1, \dots, N_n are homogeneous on $[a, b]$.

Assumption A2 may also appear very restrictive. But once again Bernoulli processes considered in (Grün et al., 1999, 2002) have the same drawback. Moreover, if necessary, one can partition $[a, b]$ in smaller intervals on which A2 is satisfied. For more precise informations on Poisson processes we refer the interested reader to (Kingman, 1993).

These assumptions are necessary in this work in order to obtain an explicit form for the expected number of coincidences (and its variance). Note that there exist some surrogate methods in the literature for which there is no need of a model on the data (see (Grün, 2009; Louis et al, 2010) for a review). In particular two kind of methods are commonly used: dithering methods (involving random shifts of individual spikes (Stark and Abeles, 2009; Louis et al., 2010), or random shifts of patterns of spikes (Harrison and Geman, 2009)), and trial-shuffling methods (Pipa et al., 2003; Pipa and Grün, 2003). However, they are based on binned coincidence count, and there is no equivalent, up to our knowledge, with a delayed coincidence count, due to serious computational issues. Alternative works have also been done in the Bayesian paradigm (Archer et al., 2013). However, as announced in the introduction, we empirically show in Section 5 that the assumptions can be weakened. In particular, point processes admitting refractory periods can be taken into account. Thus, a nice perspective of this work could be to derive theoretical results with these weakened assumptions.

3.1 Asymptotic properties

In order to build our independence test, one needs to understand the behaviour of the number of coincidence $X_{\mathcal{L}}$ under the independence hypothesis \mathcal{H}_0 . In particular, the expected value and the variance of $X_{\mathcal{L}}$ are computed here. In a general point processes framework, these computations are impossible. This is why some restrictive assumptions are needed, such as A1, A2, or the independence of the processes, as done in the original UE method where independent Bernoulli processes have been considered.

Theorem 3.1. Let \mathcal{L} and $X_{\mathcal{L}}$ be defined as previously. Assume assumptions A1 and A2 and denote by $\lambda_1, \dots, \lambda_n$ the respective intensities of N_1, \dots, N_n . Under hypothesis \mathcal{H}_0 , the expected value and the variance of the number of coincidences $X_{\mathcal{L}}$ are given by:

$$m_{0,\mathcal{L}} := \mathbb{E}[X_{\mathcal{L}}] = \left(\prod_{l \in \mathcal{L}} \lambda_l \right) I(L, 0)$$

and

$$\text{Var}(X_{\mathcal{L}}) = m_{0,\mathcal{L}} + \sum_{k=1}^{L-1} \left(\sum_{\substack{\mathcal{J} \subset \mathcal{L} \\ \#\mathcal{J}=k}} \prod_{j \in \mathcal{J}} \lambda_j^2 \prod_{l \notin \mathcal{J}} \lambda_l \right) I(L, k),$$

where the $I(L, k)$ are given by Proposition 3.1 below.

The proof relies on the calculus of the moments of a sum over a Poisson Process and is given in Appendix 8. The integral $I(L, k)$ can be seen as the contribution of a subset of k neurons to the number of coincidences between the L neurons.

Proposition 3.1. For $b > a \geq 0$ and $0 < \delta < b - a$, define for every k in $\{0, \dots, L\}$

$$I(L, k) = \int_{[a,b]^{L-k}} \left(\int_{[a,b]^k} \mathbf{1}_{\left| \max_{i \in \{1, \dots, L\}} x_i - \min_{i \in \{1, \dots, L\}} x_i \right| \leq \delta} dx_1 \dots dx_k \right)^2 dx_{k+1} \dots dx_L,$$

where the convention $\int_{[a,b]^0} f(x) dx = f(x)$ is set. Then, for $L \geq 2$, and k in $\{0, \dots, L-1\}$,

- $I(L, L) = L^2 (b - a)^2 \delta^{2L-2} - 2L(L-1)(b-a)\delta^{2L-1} + (L-1)^2 \delta^{2L}$,
- $I(L, k) = f(L, k)(b-a)\delta^{L+k-1} - h(L, k)\delta^{L+k}$,
 where $f(L, k) = \frac{k(k+1) + L(L+1)}{L-k+1}$,
 and $h(L, k) = \frac{-k^3 + k^2(2+L) + k(5+2L-L^2) + L^3 + 2L^2 - L - 2}{(L-k+2)(L-k+1)}$.

Once the behaviour of $X_{\mathcal{L}}$ under \mathcal{H}_0 is known, the method to construct an independence test is straight-forward. Suppose that M independent and identically distributed (i.i.d.) trials are given. Denote $N_i^{(k)}$ the spike train corresponding to the neuron i during the k^{th} trial. As for the UE method, the idea is to compare two estimates of the expectation of $X_{\mathcal{L}}$. The first one is the empirical mean of $X_{\mathcal{L}}$:

$$\bar{m}_{\mathcal{L}} = \frac{1}{M} \sum_{k=1}^M X_{\mathcal{L}}^{(k)}, \quad (3)$$

where $X_{\mathcal{L}}^{(k)}$ is the delayed coincidence count during the k^{th} trial. This estimate converges even if the processes are not independent. More precisely the following asymptotic result is given by the Central Limit Theorem

$$\sqrt{M}(\bar{m}_{\mathcal{L}} - \mathbb{E}[X_{\mathcal{L}}]) \xrightarrow[M \rightarrow \infty]{\mathcal{D}} \mathcal{N}(0, \mathbf{Var}(X_{\mathcal{L}})),$$

where $\xrightarrow{\mathcal{D}}$ denotes the convergence of distribution and $\mathcal{N}(\mu, \sigma^2)$ denotes the Gaussian distribution with mean μ and variance σ^2 .

The second estimate is given by Theorem 3.1. Indeed, under \mathcal{H}_0 the following equality holds

$$\mathbb{E}[X_{\mathcal{L}}] = m_{0,\mathcal{L}} = \left(\prod_{l \in \mathcal{L}} \lambda_l \right) I(L, 0).$$

Replacing each spiking intensity λ_l by

$$\hat{\lambda}_l := \frac{1}{M(b-a)} \sum_{k=1}^M N_l^{(k)}([a, b]),$$

where $N_l^{(k)}([a, b])$ denotes the number of spikes in $[a, b]$ for neuron l during the k^{th} trial, gives the following estimator,

$$\hat{m}_{0,\mathcal{L}} = \left(\prod_{l \in \mathcal{L}} \hat{\lambda}_l \right) I(L, 0). \quad (4)$$

Note that $\bar{m}_{\mathcal{L}}$ is always consistent (that is, converges towards the true parameter) whereas $\hat{m}_{0,\mathcal{L}}$ is consistent only under \mathcal{H}_0 . This leads to the following independence test: the independence assumption is rejected when the difference between $\bar{m}_{\mathcal{L}}$ and $\hat{m}_{0,\mathcal{L}}$ is too large. More precisely, Theorem 3.2 gives the asymptotic behaviour of $\sqrt{M}(\bar{m}_{\mathcal{L}} - \hat{m}_{0,\mathcal{L}})$ under \mathcal{H}_0 .

Theorem 3.2. *Under the notations and assumptions of Theorem 3.1, and under \mathcal{H}_0 , the following affirmations are true*

- *The following convergence of distribution holds:*

$$\sqrt{M}(\bar{m}_{\mathcal{L}} - \hat{m}_{0,\mathcal{L}}) \xrightarrow[M \rightarrow \infty]{\mathcal{D}} \mathcal{N}(0, \sigma^2),$$

with

$$\sigma^2 = \mathbf{Var}(X_{\mathcal{L}}) - (b-a)^{-1} \mathbb{E}[X_{\mathcal{L}}]^2 \left(\sum_{l \in \mathcal{L}} \lambda_l^{-1} \right).$$

- Moreover, σ^2 can be estimated by

$$\hat{\sigma}^2 = \hat{v}(X_{\mathcal{L}}) - (b - a)^{-1} I(L, L) \prod_{l \in \mathcal{L}} \hat{\lambda}_l^2 \left(\sum_{l \in \mathcal{L}} \hat{\lambda}_l^{-1} \right),$$

where

$$\hat{v}(X_{\mathcal{L}}) = \hat{m}_{0,\mathcal{L}} + \sum_{k=1}^{L-1} \left(\sum_{\substack{\mathcal{J} \subset \mathcal{L} \\ \#\mathcal{J}=k}} \prod_{j \in \mathcal{J}} \hat{\lambda}_j^2 \prod_{l \notin \mathcal{J}} \hat{\lambda}_l \right) I(L, k),$$

and the following convergence of distribution holds:

$$\sqrt{M} \frac{(\bar{m}_{\mathcal{L}} - \hat{m}_{0,\mathcal{L}})}{\sqrt{\hat{\sigma}^2}} \xrightarrow{\mathcal{D}} \mathcal{N}(0, 1).$$

The proof of this theorem relies on a standard application of the delta method (Casella and Berger, 2002) and is given in Appendix 8.2. The delta method is useful in order to deal with the plug-in step, i.e. the substitution of the real parameters by the estimated ones.

Note that the results obtained in Theorems 3.1 and 3.2 are true for more general delayed coincidence counts. A more general result and its proof are given in Appendix. However when one considers more general ways to count coincidences the integrals $I(L, k)$ are harder to compute.

3.2 Independence test

The results obtained in Theorem 3.2 allow us to straightforwardly build a test for detecting a dependency between neurons:

Definition 3.1 (The GAUE test). *For α in $]0, 1[$, denote z_{α} the α -quantile of the standard Gaussian distribution $\mathcal{N}(0, 1)$. Then the symmetric test of level α rejects \mathcal{H}_0 when \bar{m} and $\hat{m}_{0,\mathcal{L}}$ are too different, that is when*

$$\left| \sqrt{M} \frac{(\bar{m}_{\mathcal{L}} - \hat{m}_{0,\mathcal{L}})}{\sqrt{\hat{\sigma}^2}} \right| > z_{1-\alpha/2}.$$

Note that once a subset is rejected by our test, one can determine if the dependency is rather excitatory or inhibitory according to the sign of $\bar{m}_{\mathcal{L}} - \hat{m}_{0,\mathcal{L}}$. If $\bar{m}_{\mathcal{L}} - \hat{m}_{0,\mathcal{L}} > 0$ (respectively < 0) then the dependency is rather excitatory (respectively inhibitory).

The result of a test may be wrong in two distinct manners. On the one hand, a false positive is an error in which the test is incorrectly rejecting the null hypothesis. On the other hand, a false negative is an error in which the test is incorrectly accepting the null hypothesis. The false positive (respectively negative) rate is the test's probability that a false positive (resp. negative) occurs. Usually, a theoretical control is given only for the false positive rate which is considered as the worst error. The following corollary is an immediate consequence of Theorem 3.2 and states the appropriateness of the GAUE test.

Corollary 3.1. *Under assumptions of Theorem 3.2, the test of level α presented in Definition 3.1 is asymptotically of false positive rate α . That is, the false positive rate of the test tends to α when the sample size M tends to infinity.*

4 Illustration Study: Poissonian Framework

In this section, an illustration of the previous theoretical results is given. To obtain a global evaluation of the performance of the different methods, some parameters can randomly fluctuate. More precisely, the following procedure is applied,

1. Generate a set of random parameters according to the appropriate Framework;
2. Use this set to generate M trials;
3. Compute the different statistics;
4. Repeat steps 1 to 3 a thousand times.

} **P**

We begin by an illustration of the results of Theorem 3.2 and Corollary 3.1, and a comparison with the original UE method.

4.1 Illustration of the asymptotic properties

The control on the false positive rate of our test being only asymptotic, it is evaluated on simulations in this Section. Moreover, it is shown that our test is empirically *conservative*, that is, when constructed for a prescribed level, say α , the empirical false positive rate is less than α . We simulate independent Poisson processes under the following Framework (**F**₁) :

- the trial duration $(b - a)$ is randomly selected (uniform distribution) between 0.2s and 0.4s;
- the $n = 4$ neurons are simulated with different intensities. Each one is randomly selected (uniform distribution) between 8 and 20Hz;
- the set of tested neurons is given by $\mathcal{L} = \{1, 2, 3, 4\}$;

} **F**₁

Moreover, we set once and for all $\delta = 0.01s$. Note that the dependence with respect to the parameter δ has been fully discussed in (Albert et al., 2014).

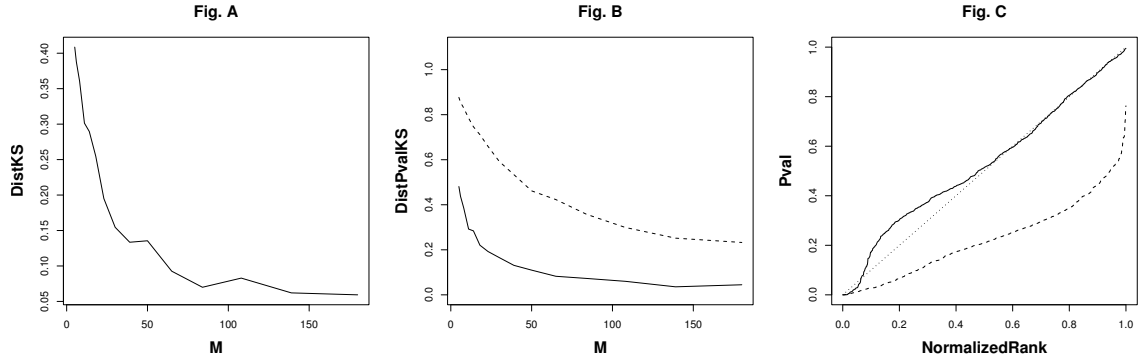


Figure 2: Under Framework **F**₁ (Independence assumption). **Figure A.** Evolution of the Kolmogorov distance (in function of the number of trials) averaged on 1000 simulations between the empirical distribution function of the test statistics and the standard Gaussian distribution function. **Figure B.** Evolution of the Kolmogorov distance averaged on 1000 simulations between the empirical distribution function of the p-values and the uniform distribution function with respect to the number of trials. The plain line stands for our test and the dashed line for the original UE one. **Figure C.** Graphs of the sorted 1000 p-values (for 50 trials) in function of their normalized rank under \mathcal{H}_0 . The plain line stands for our test, the dashed line for the original UE one and the dotted line for the uniform distribution function.

Considering M independent trials of n point processes, the asymptotic (with respect to M) of the delayed coincidence count is studied. To this aim, we use a Monte Carlo method following the procedure **P** presented at the beginning of Section 4. On each simulation, M independent trials are generated and the statistic $S_i = \sqrt{M}(\bar{m}_{\mathcal{L},i} - \hat{m}_{0,i}) / \sqrt{\hat{\sigma}_i^2}$ (for i from 1 to 1000) is computed.

Theorem 3.2 tells us that the random variables S_i should be asymptotically distributed as the standard Gaussian distribution. Thus, we plot (Figure 2.A) the Kolmogorov distance $KS(F_{M,1000}, F)$ between the empirical distribution function over the 1000 repetition $F_{M,1000}$ and the standard Gaussian distribution function F :

$$KS(F_{M,1000}, F) = \sup_x |F_{M,1000}(x) - F(x)|.$$

Usually, a test of level $\alpha = 0$ always accepts, whereas a test of level $\alpha = 1$ always rejects. Hence, there is a critical value (depending on the observations, and called p-value) for which the test decision passes from acceptance to rejection. If the false positive rate of a test of level α is exactly α for all α in $[0, 1]$, which should asymptotically be the case according to Corollary 3.1, then one can prove that the corresponding p-value is uniformly distributed on $[0, 1]$ under the null hypothesis. Thus, the evolution (with respect to M) of the Kolmogorov distance between the empirical distribution function of the obtained p-values (with our test and the one given by the UE method) and the uniform distribution function is plotted for symmetric tests (See Figure 2.B). It appears that the rate of convergence of the empirical distribution function of the p-values is faster for our test than the one given by the UE method.

From Figures 2.A and B, it seems reasonable to consider, for our test, sample sizes M greater than 50. Indeed, one sees that the distribution of our statistic is then almost Gaussian and the distribution of the p-values almost uniform (as expected under the null hypothesis). Thus, in order to describe more precisely what happens, we plot in Figure 2.C the sorted p-values in function of their normalized rank for $M = 50$. Note that if the curve of sorted p-values is below (respectively above) the diagonal, then the observed p-values are globally smaller (respectively greater) than they should be under \mathcal{H}_0 . Our test seems to be conservative except for big or very small p-values. The problem induced by this non conservativeness for very small p-values is detailed at the end of Section 5. On the other side, the false positive rate observed for the UE test is too high. For example, we see in the figure that the UE test with a theoretical test level of 5% rejects almost 20% of the cases.

4.2 Parameter Scan

Here is illustrated the influence of the parameters λ (the firing rate) and $b - a$ (the trial duration). We plot in Figure 3 the evolution (with respect to M) of the Kolmogorov distance between the empirical distribution function of the obtained p-values (with our test and the one given by the UE method) and the uniform distribution function.

First of all, note that, if the Kolmogorov distance between the empirical distribution function of the obtained p-values and the uniform distribution function tends to 0, then it means that the false positive rate of the test of level α tends to α when the sample size tends to infinity. As predicted by Corollary 3.1, the Kolmogorov distance between the empirical distribution function of the obtained p-values with our test tends to 0 fast enough if λ is not too small ($\lambda \geq 15\text{Hz}$). The test induced by the UE method seems to share the same asymptotic behaviour, but with a slower rate of convergence. Finally, it seems that our method performs better than the UE method in all the configurations of parameters.

In order to describe more precisely what happens, we plot in Figure 4 the sorted p-values in function of their normalized rank (for $M = 50$). As expected in regard of Figure 3, the plain line sticks to the first diagonal when the parameters are large enough, since, in those cases, the KS distance between the empirical distribution function of the p-values of our test and the uniform distribution function was already small for $M = 50$. However, the test induced by the UE method does not respect the prescribed level even when the parameters are large. Indeed, the dashed line remains under the diagonal in all cases. Thus, even if the asymptotic level of the UE method is good, in the practical cases where the sample size is small, the false positive rate is not guaranteed.

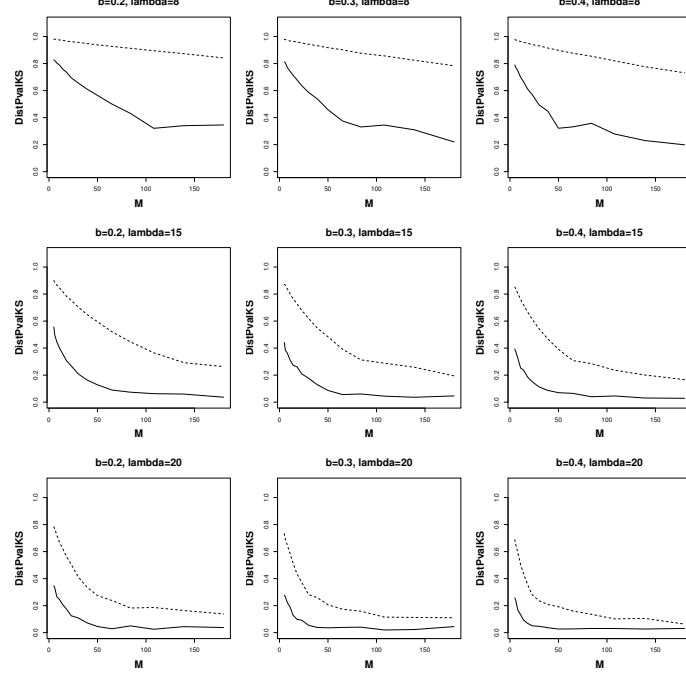


Figure 3: Under Framework \mathbf{F}_1 (Independence assumption). Evolution of the Kolmogorov distance averaged on 1000 simulations between the empirical distribution function of the p-values and the uniform distribution function with respect to the number of trials. The plain line stands for our test and the dashed line for the original UE one. Each plot stands for different values of λ and b (we set $a = 0$ so that b gives the trial duration $b - a$). From top to bottom λ takes the values 8, 15 and 20Hz. From left to right, b takes the values 0.2, 0.3 and 0.4s.

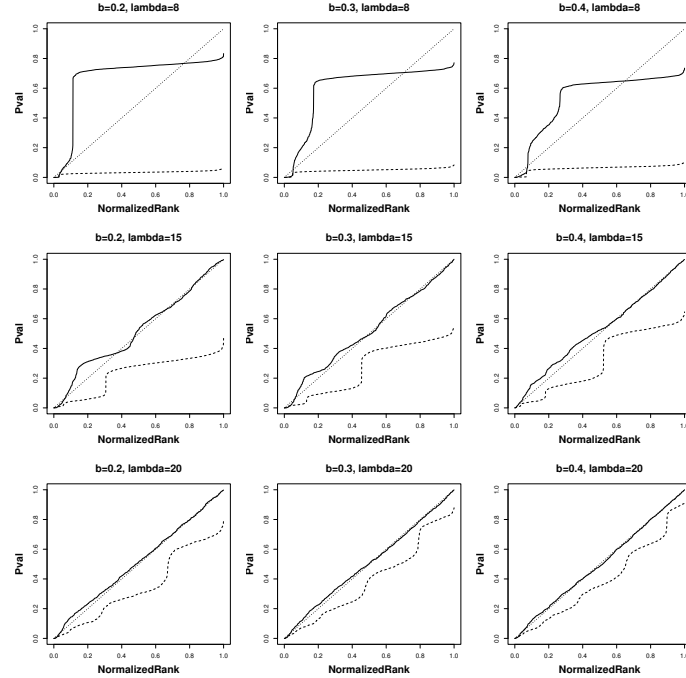


Figure 4: Under Framework \mathbf{F}_1 (Independence assumption). Graphs of the sorted 1000 p-values (for 50 trials) in function of their normalized rank under \mathcal{H}_0 . The plain line stands for our test, the dashed line for the original UE one and the dotted line for the uniform distribution function. Each plot stands for different values of λ and b (we set $a = 0$ so that b gives the trial duration $b - a$). From top to bottom λ takes the values 8, 15 and 20Hz. From left to right, b takes the values 0.2, 0.3 and 0.4s.

4.3 Illustration of the true positive rate

First, let us note that the *true positive rate* of a test is the test's probability of correctly rejecting the null hypothesis. No theoretical result on this rate can be obtained from Theorem 3.2 who deals only with the false positive rate. So, in order to evaluate the true positive rate of the test, we simulate a sample which is dependent and check how many times the test rejects \mathcal{H}_0 .

To obtain dependent Poisson processes an injection model inspired by the one used in (Grün et al., 2002, 1999) or (Tuleau-Malot et al., 2014) is used. Consider independent homogeneous Poisson processes $\bar{N}_1, \dots, \bar{N}_n$, drawn according to Framework \mathbf{F}_1 . Then, simulate an other Poisson process (according to the same framework but independent from the previous ones) \tilde{N} , with an intensity of 0.3Hz, which is injected to every neuron. Thus our sequence of dependent Poisson processes is given by

$$N_i = \bar{N}_i \cup \tilde{N}.$$

This new framework (\mathbf{F}_1 completed by the injection) is referred as Framework \mathbf{F}_2 .

Note that this injection model can only model excess of coincidences and not lack of coincidences. In the injection model used in (Grün et al., 1999), a small jitter is applied before injection to mimic temporal imprecision of the synchronous event. In our Poissonian framework this jitter cannot be performed in a similar way. Indeed, this jitter does not preserve the stationariness of the Poisson process near the edges. Although some other more elaborate injection models are available in the Poissonian framework, we do not use one of them here because their translation in the discrete time framework is not clear.

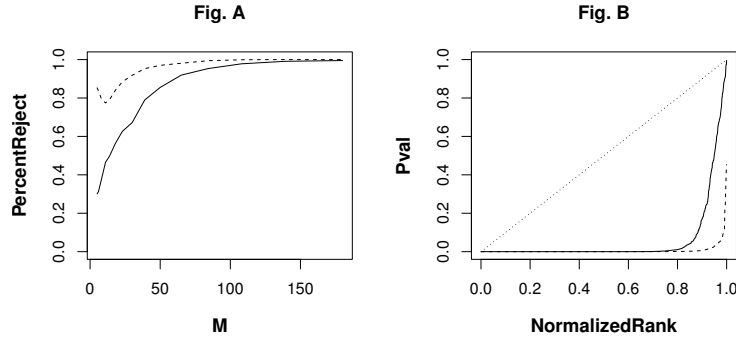


Figure 5: Under Framework \mathbf{F}_2 (Dependence assumption). **Figure A.** Illustration of the true positive rate of the test, for a theoretical test level of 5%. The curves represent the evolution, with respect to the number of trials, of the true positive rate (averaged on 1000 simulations). The plain line stands for our test and the dashed line for the original UE one. **Figure B.** Graphs of the sorted 1000 p-values for dependent Poisson processes (50 trials). The plain line stands for our test, the dashed line for the original UE one and the dotted line for the uniform distribution function.

For a fixed theoretical level of $\alpha = 5\%$, Figure 5.A illustrates the true positive rate of the two tests in function of the number of trials M . Then Figure 5.B represents the p-values as a function of their normalized rank, for $M = 50$. As in Figure 2.C, the lower the curve is, the greater the observed frequency of rejection of the null hypothesis. The true positive rate is higher for the UE method for small sample sizes, but this is at the price of an undervalued theoretical level. Indeed, we saw previously (Section 4.1) that the UE test gives too much false positives (for $M = 50$, 20% of rejection under the null hypothesis with a theoretical test level of 5%).

5 Illustration Study: Non-Poissonian framework

In this section, a more neurobiologically realistic framework than the Poisson one is considered. Indeed, it is interesting to see if our test is still reliable when the Poisson framework is not valid any-more. Our test is confronted to multivariate Hawkes processes, which can be simulated thanks to Ogata's thinning method (Ogata, 1981) inspired by (Lewis and Shedler, 1979). The use of

Hawkes processes in neurobiology was first introduced in (Chornoboy et al., 1988). With the development of simultaneous neuron recordings there is a recent trend in favour of Hawkes processes for modelling spike trains ((Pillow et al., 2008; Krumin et al., 2010; Pernice et al., 2011, 2012; Tuleau-Malot et al., 2014)). Furthermore, Hawkes processes have passed some goodness-of-fit tests on real data (Reynaud-Bouret et al., 2014). In this model, interaction between two neurons can be easily and in a more realistic way inserted. This is one of the reasons of this trend. Note that the homogeneous Poisson process is a particular case of Hawkes processes, with no interaction between neurons.

A counting process N is characterized by its conditional intensity λ_t which is related with the local probability of finding a new point given the past. (Informally, the quantity $\lambda_t dt$ gives the probability that a new point on N appears in $[t, t + dt]$ given the past). The process $(N^i)_{i=1\dots n}$ is a multivariate Hawkes process if there exist some functions $(h_{ij})_{i,j=1\dots n}$ (called interaction functions) and some positive constants $(\mu_i)_{i=1\dots n}$ (spontaneous intensities) such that, for all $j = 1, \dots, n$, λ^j given by

$$\lambda_t^j = \max \left(0, \mu_j + \sum_{i=1}^n \int_{s < t} h_{ij}(t-s) N^i(ds) \right)$$

is the intensity of the point process N^j , where $N^i(ds)$ is the point measure associated to N^i , that is $N^i(ds) = \sum_{T \in N^i} \delta_T(ds)$ where δ_T is the Dirac measure at point T .

The functions h_{ij} represent the influence of neuron i over neuron j in terms of spiking intensity. This influence can be either exciting ($h \geq 0$) or inhibiting ($h \leq 0$). For example, suppose that $h_{ij} = \beta \mathbf{1}_{[0,x]}$. If $\beta > 0$ (respectively $\beta < 0$) then the apparition of a spike on N^i increases (respectively decreases) the probability to have a spike on N^j during a short period of time (namely x): neuron i excites (respectively inhibits) neuron j . The processes N^i for $i = 1, \dots, n$ are independent if and only if $h_{ij} = 0$ for all $i \neq j$.

Note also that the self-interaction functions h_{jj} can model refractory periods, making the Hawkes model more realistic than Poisson processes, even in the independence case. In particular when $h_{jj} = -\mu_j \mathbf{1}_{[0,x]}$, all the other interaction functions being null, the n -dimensional process is composed by n independent Poisson processes with dead time x , modelling strict refractory periods of length x (Reimer et al., 2012).

All the following tests are computed according to the Framework **F**₃ below:

- the trial duration of $b - a$ is randomly selected (uniform distribution) between 0.2 and 0.4s;
- the $n = 4$ neurons are simulated with spontaneous intensity μ_1, \dots, μ_4 randomly selected (uniform distribution) between 8 and 20Hz;
- the non-positive auto interaction functions are given by $h_{i,i} = -\mu_i \mathbf{1}_{[0,0.003s]}$;
- the set of tested neurons is given by $\mathcal{L} = \{1, 2, 3, 4\}$;

F₃

We also performed a parameter scan. However, since the results are equivalent to those obtained in the Poissonian framework, they are not presented here.

5.1 Illustration of the level

Before all, one wants to know if Theorem 3.2 and Corollary 3.1 are still reliable for Hawkes processes. Thus as in section 4, Figure 6.A shows the evolution of the KS distance between $F_{M,1000}$ and F . Then as in Section 4, we look at the KS distance between the empirical distribution function of the p-values and the uniform distribution function to see if one can trust the level of the different tests (Figure 6.B). These two figures are pretty similar to Figures 2.A and B (Poissonian case), but with a slightly slower convergence rate (with respect to M). Finally, Figure 6.C plays the same role as Figure 2.C and presents the sorted p-values in function of their normalized rank

(for $M = 50$). Again, the results are comparable to those obtained in the Poissonian case: our test is rather conservative whereas the UE test rejects too many cases.

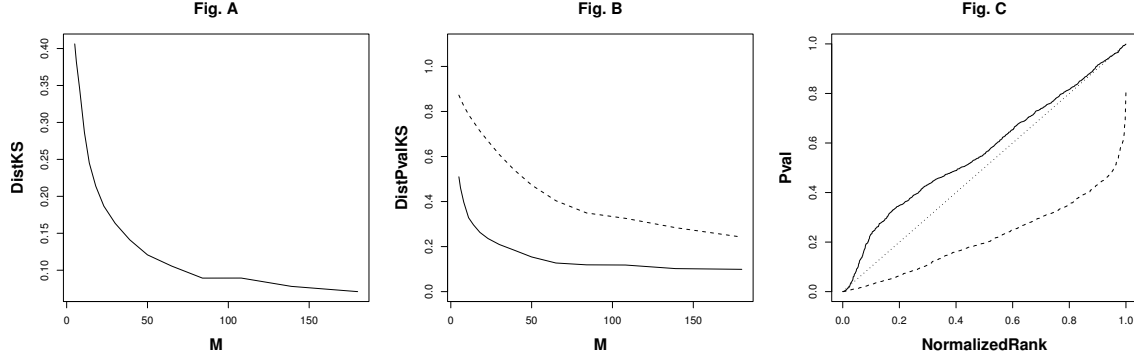


Figure 6: Under Framework \mathbf{F}_3 (Independence assumption). **Figure A.** Evolution of the Kolmogorov distance (in function of the number of trials) averaged on 1000 simulations between the empirical distribution function of the test statistics and the standard Gaussian distribution function. **Figure B.** Evolution of the Kolmogorov distance averaged on 1000 simulations between the empirical distribution function of the p-values and the uniform distribution function with respect to the number of trials. The plain line stands for our test and the dashed line for the original UE one. **Figure C.** Graphs of the sorted 1000 p-values (for 50 trials) in function of their normalized rank under \mathcal{H}_0 . The plain line stands for our test, the dashed line for the original UE one and the dotted line for the uniform distribution function.

5.2 Illustration of the true positive rate

As said previously, it is more realistic to introduce dependency between Hawkes processes than Poisson processes. Still considering Framework \mathbf{F}_3 , interaction functions $h_{i,j} = \beta \mathbf{1}_{[0,0.005s]}$, β being randomly selected between 20 and 30 Hz, are added. More precisely, we add five interaction functions: $h_{1,3}$, $h_{2,3}$, $h_{1,4}$, $h_{2,4}$ and $h_{3,4}$ (summarized in Figure 7). Moreover, the auto interactions are updated to preserve strict refractory periods : $h_{i,i} = -(\mu_i + m_i \cdot \beta) \mathbf{1}_{[0,0.003s]}$, where m_i is the number of neurons exciting neuron i (for example, $m_4 = 3$). This new framework (\mathbf{F}_3 completed by the five interaction function) is referred as Framework \mathbf{F}_4 .

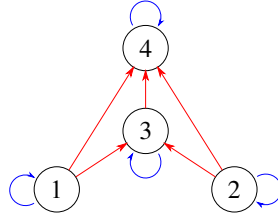


Figure 7: Local independence graph. An arrow means a non null interaction function. Blue arrow means inhibition and red arrow means excitation.

As previously we first provide an illustration of the true positive rate of the two tests, associated to a theoretical level of 5%, in function of M (Figure 8.A). Then Figure 8.B represents the p-values in function of their normalized rank, for $M = 50$. The difference between the true positive rates is smaller than in the Poissonian Case.

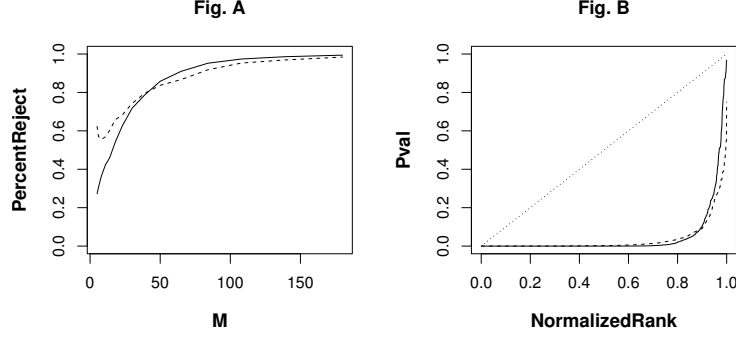


Figure 8: Under Framework \mathbf{F}_4 (Dependence assumption, see Figure 7). **Figure A.** Illustration of the true positive rate of the test, for a theoretical test level of 5%. The curves represent the evolution, with respect to the number of trials, of the true positive rate (averaged on 1000 simulations). The plain line stands for our test and the dashed line for the original UE one. **Figure B.** Graphs of the sorted 1000 p-values for 50 trials. The plain line stands for our test, the dashed line for the original UE one and the dotted line for the uniform distribution function.

5.3 Multiple pattern test

In the original MTGAUE method, a multiple testing procedure is applied with respect to 1900 sliding time windows. In our framework, we cannot guarantee the relevance of the multiple test with this high order of multiplicity. This is due to the default of the Gaussian approximation and, more precisely, to the excess of very small p-values as noted in Section 4.1. But, we are able to propose a multiple testing procedure with respect to the different possible patterns. For example, with four neurons there are eleven different possible patterns, which gives a much lower order of multiplicity. So, the multiple test over all the eleven sub-pattern of two, three or four neurons is presented here.

In multiple testing, the notion of false positive rate is not relevant. The closest notion might be the *Family-Wise Error Rate* (FWER) which is the probability to wrongly reject at least one of the tests. This error rate can be controlled using Bonferroni's method but it is too restrictive, in particular when the number K of tests involved is too large. One popular way to deal with multiple testing is the Benjamini-Hochberg procedure (Benjamini and Hochberg, 1995) which ensures a control of the *False Discovery Rate* (FDR). False discoveries cannot be avoided but it is not a problem if the ratio of F_p (the number of false positives detections) divided by R (the total number of rejects) is controlled. Therefore, the FWER and the FDR are mathematically defined by $\text{FWER} = \mathbb{P}(F_p > 0)$ and $\text{FDR} = \mathbb{E}[F_p/R \mathbf{1}_{R>0}]$.

Note that in the full independent case, the FWER and the FDR are equal. The following procedure, due to Benjamini and Hochberg ensures a small FDR over K tests:

1. Fix a level q ($q = 5\%$ for example);
2. Denote by (P_1, \dots, P_K) the p-values obtained for all considered tests;
3. Order them in increasing order and denote the increasing vector $(P_{(1)}, \dots, P_{(K)})$;
4. Note k_0 the largest k such that $P_{(k)} \leq kq/K$;
5. Then, reject all the tests corresponding to p-values smaller than $P_{(k_0)}$.

The theoretical result of (Benjamini and Hochberg, 1995) ensures that if the p-values are upper bounded by a uniform distribution and independently distributed under the null hypothesis, then the procedure guarantees a FDR less than q . The main drawback of this procedure in our case is that one needs to compute p-values that are very small when K is large. For example, if $K \geq 50$ and $q = 5\%$, the upper bound given by kq/K can be smaller than 0.001 and as noted in Section 4.1 the empirical frequency of very small p-values is greater than expected and therefore the uniform upper bound of the p-values is not guaranteed in our case. However, only 11 tests are considered

here and the procedure still returns reliable results.

We perform 1000 simulations and count how many times each test rejects the independence. The results, obtained for $M = 50$, are presented in Figure 9.

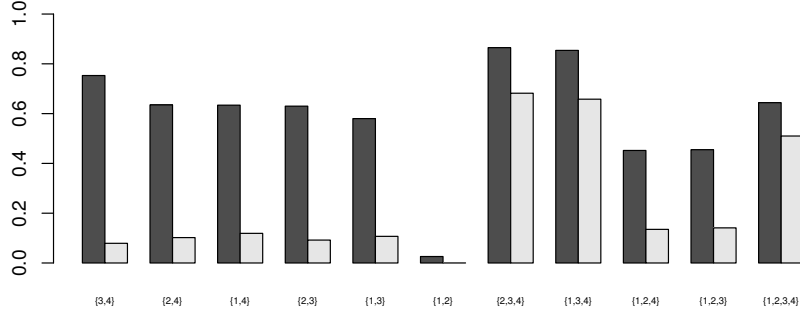


Figure 9: Under Framework \mathbf{F}_4 (Dependence assumption, see Figure 7). Frequency of dependence detections (1000 simulations) for each pattern. Grey for our test, white for the original UE method.

The results show that our test detects all patterns except $\{1, 2\}$. This is consistent with the considered framework (\mathbf{F}_4) since we simulate connections between all pairs of neurons except $\{1, 2\}$. The U.E. test essentially detects the patterns $\{2, 3, 4\}$, $\{1, 3, 4\}$, $\{1, 2, 3, 4\}$ and to a lesser extent $\{1, 2, 4\}$ and $\{1, 2, 3\}$. Moreover, it misses all the pairs.

6 Illustration on real data

After validating our test on simulations, we apply our method on real data and show results in agreement with classical knowledge on those data.

6.1 Description of the data

The data set considered here is the same as in (Tuleau-Malot et al., 2014) and previous experimental studies (Grammont and Riehle, 2003; Riehle et al., 2000, 2006). The following description of the experiment is copied from Section 4.1 of (Tuleau-Malot et al., 2014). These data were collected on a 5-year-old male Rhesus monkey who was trained to perform a delayed multi-directional pointing task. The animal sat in a primate chair in front of a vertical panel on which seven touch-sensitive light-emitting diodes were mounted, one in the center and six placed equidistantly (60 degrees apart) on a circle around it. The monkey had to initiate a trial by touching and then holding with the left hand the central target. After a fix delay of 500ms, the preparatory signal (PS) was presented by illuminating one of the six peripheral targets in green. After a delay of either 600ms (with probability 0.3) or 1200ms (with probability 0.7), it turned red, serving as the response signal and pointing target. Signals recorded from up to seven micro-electrodes (quartz insulated platinum-tungsten electrodes, impedance: 2-5M Ω at 1000Hz) were amplified and band-pass filtered from 300Hz to 10kHz. Using a window discriminator, spikes from only one single neuron per electrode were then isolated. Neuronal data along with behavioural events (occurrences of signals and performance of the animal) were stored on a PC for off-line analysis with a time resolution of 10kHz. The idea of the analysis is to detect some conspicuous patterns of coincident spike activity appearing during the response signal in the case of a long delay (1200ms). Therefore, we only consider trials where the response signal is indeed occurring after a long delay.

6.2 The test

We have at hand the following data: spike trains associated to four neurons (35 trials by neurons). We consider two sub windows: one between 300ms and 500ms (i.e. before the preparatory signal),

the other between 1100ms and 1300ms (i.e. around the expected signal). Our idea is that more synchronisation should be detected during the second window. Moreover, we do not only want to test if the four considered neurons are independent (that is perform our test on the complete pattern $\{1, 2, 3, 4\}$). Indeed one can be interested in knowing if neurons in some sub-patterns (for example $\{1, 2\}$ or $\{1, 3, 4\}$ are independent. That is why we use the multiple pattern test procedure defined at the end of Section 5 to test all the eleven subsets (of at least two neurons) of the four considered neurons are tested. Thus we use the Benjamini-Hochberg procedure (presented in the previous section) for $K = 22$ tests. Moreover, we took several values for the delay δ between 0.01s and 0.025s and the results remained stable.

The results are presented in Figure 10. Note that we saw in sections 4 and 5 that our test is too conservative even for small number of trials. This ensures that the theoretical level of our test can be trusted. We see that synchronizations between the subsets $\{3, 4\}$ and $\{1, 3, 4\}$ appear in the second window. These results suggest that neurons 1, 3 and 4 belong to a neuronal assembly which is formed around the expected signal. This is in agreement with more quantitative results on those data (Grammont and Riehle, 2003; Tuleau-Malot et al., 2014).



Figure 10: Evolution of the synchronization between neurons. The lines indicate the subset for which our test detects dependence. Here we detect an excess of coincidences between neurons $\{1, 3, 4\}$ and $\{3, 4\}$

7 Conclusion

This paper generalizes the statistical study of the delayed coincidence count performed in (Tuleau-Malot et al., 2014) to more than two neurons. This delayed coincidence count leads to an independence test for point processes which are commonly used to model spike trains.

Under the hypothesis that the point processes are homogeneous Poisson processes, the expectation and variance of the delayed coincidence count can be computed (Theorem 3.1), and then a test with prescribed asymptotic level is built (Theorem 3.2). A simulation study allows us to confirm our theoretical results and to state the empirical validity of our test with a relaxed Poisson assumption. Indeed, we considered Hawkes processes which are a more realistic model of spike trains. The simulation study gives good results, even for small sample size. This allows us to use our test on real data, in order to highlight the emergence of a neuronal assembly involved at some particular time of the experiment.

We achieved the full generalization of the single test procedure introduced in (Tuleau-Malot et al., 2014). However, we could not achieve the multiple time windows testing procedure mainly because of the default of Gaussian approximation concerning extreme values of the test statistics. More precisely, very small p-values are not distributed as expected. In particular, as noted at the end of Section 4.1, when the sample size M is moderate ($M = 50$), our test returns too many very small p-values. In (Tuleau-Malot et al., 2014), the MTGAUE method is applied simultaneously on 1900 sliding windows. In the present work, in order to apply multiple testing both with respect to the sliding time windows and the subsets, the total number of tests is even larger. Indeed, for each

sliding window, there are $2^n - n - 1$ tests to perform, where n is the number of recorded neurons. As said at the end of Section 5 this would lead to extremely small p-values, for which our test is less reliable.

Even if our test remains empirically reliable under a non Poissonian framework, it could be therefore of interest to explore surrogate data method such as trial-shuffling (Pipa et al., 2003). A very recent work based on permutation approach for delayed coincidence count with $n = 2$ neurons (Albert et al., 2014) is a first step in this direction but needs to be generalized to more than 2 neurons.

Acknowledgements

We first of all want to thank Alexa Riehle, leader of the laboratory in which the data used in this article were previously collected, and Franck Grammont who collected these data. Finally we thank Patricia Reynaud-Bouret for fruitful discussions.

8 Proofs

As said in Section 3.1, we prove more general results than Theorems 3.1 and 3.2. Considering N_1, \dots, N_n , some point processes on $[a, b]$ and $\mathcal{L} \subset \{1, \dots, n\}$ a set of indices with cardinal $L \geq 2$, we prove the same kind of results with any coincidence function $c(x_1, \dots, x_L)$ with value either 0 or 1 satisfying Definition 8.1 below.

Definition 8.1.

1. A coincidence function is a function $c : [a, b]^L \rightarrow \{0, 1\}$ which is symmetric.
2. Let $(x_1, \dots, x_L) \in \prod_{l \in \mathcal{L}} N_l$ be a L -tuple with a spiking time of every neuron of the subset \mathcal{L} . Say that (x_1, \dots, x_L) is a coincidence if and only if $c(x_1, \dots, x_L) = 1$.
3. Given c a coincidence function, we define $X_{\mathcal{L}}$ the number of coincidences on $[a, b]$ by:

$$X_{\mathcal{L}} = \sum_{(x_1, \dots, x_L) \in \prod_{l \in \mathcal{L}} N_l} c(x_1, \dots, x_L).$$

4. Define

$$\forall k \in \{0, \dots, L\}, I(L, k) = \int_{[a, b]^{L-k}} \left(\int_{[a, b]^k} c(x_1, \dots, x_L) dx_1 \dots dx_k \right)^2 dx_{k+1} \dots dx_L$$

where the convention $\int_{[a, b]^0} f(x) dx = f(x)$ is set.

8.1 Proof of Theorem 3.1

Theorem 8.1. Under assumptions and notations of Definition 8.1, if N_1, \dots, N_n are some independent homogeneous Poisson processes on $[a, b]$ with intensities $\lambda_1, \dots, \lambda_n$, the expected value and the variance of the number of coincidences $X_{\mathcal{L}}$ are given by:

$$m_{0, \mathcal{L}} := \mathbb{E}[X_{\mathcal{L}}] = \left(\prod_{l \in \mathcal{L}} \lambda_l \right) I(L, 0) \quad (5)$$

and

$$\text{Var}(X_{\mathcal{L}}) = m_{0, \mathcal{L}} + \sum_{k=1}^{L-1} \left(\sum_{\substack{\mathcal{J} \subset \mathcal{L} \\ \#\mathcal{J}=k}} \prod_{j \in \mathcal{J}} \lambda_j^2 \prod_{l \notin \mathcal{J}} \lambda_l \right) I(L, k). \quad (6)$$

Proof. By definition,

$$\mathbb{E}[X_{\mathcal{L}}] = \mathbb{E} \left[\sum_{(x_1, \dots, x_L) \in \prod_{l \in \mathcal{L}} N_l} c(x_1, \dots, x_L) \right].$$

Using the fact that N_1, \dots, N_n are independent homogeneous Poisson processes with respective intensities $\lambda_1, \dots, \lambda_n$ one can prove (see (Daley and Vere-Jones, 2003)) that

$$\mathbb{E}[X_{\mathcal{L}}] = \left(\prod_{l \in \mathcal{L}} \lambda_l \right) \int_{[a, b]^L} c(x_1, \dots, x_L) dx_1 \dots dx_L = \left(\prod_{l \in \mathcal{L}} \lambda_l \right) I(L, 0).$$

For sake of simplicity, the variance is computed in the simpler case where $\mathcal{L} = \{1, \dots, L\}$, the generalization being pretty clear. In order to simplify, we use the integral form of the coincidence count, i.e.

$$X_{\mathcal{L}} = \int_{[a, b]^L} c(x_1, \dots, x_L) dN_1(x_1) \dots dN_L(x_L)$$

where dN_1, \dots, dN_L are the point measures associated to N_1, \dots, N_L . Thanks to Fubini Theorem we have

$$\mathbb{E}[X_{\mathcal{L}}^2] = \mathbb{E} \left[\int_{[a,b]^{2L}} c(x_1, \dots, x_L) c(y_1, \dots, y_L) \prod_{l=1}^L dN_l(x_l) dN_l(y_l) \right]. \quad (7)$$

Then, let us define

$$[a, b]^{(1)} = \{(x, y) \in [a, b]^2 \mid x = y\} \text{ and } [a, b]^{(2)} = [a, b]^2 \setminus [a, b]^{(1)}. \quad (8)$$

Now, let us see that $[a, b]^{2L} = ([a, b]^2)^L = \sqcup_{\varepsilon \in \{1,2\}^L} \left(\prod_{l=1}^L [a, b]^{(\varepsilon_l)} \right)$ where ε_l denotes the l -th coordinate of ε . Using this decomposition and Equation (7), it is clear that

$$\mathbb{E}[X_{\mathcal{L}}^2] = \sum_{\varepsilon \in \{1,2\}^L} A_{\varepsilon}, \quad (9)$$

where for all ε in $\{1, 2\}^L$,

$$A_{\varepsilon} = \mathbb{E} \left[\int_{\prod_{l=1}^L [a, b]^{(\varepsilon_l)}} c(x_1, \dots, x_L) c(y_1, \dots, y_L) \prod_{l=1}^L dN_l(x_l) dN_l(y_l) \right].$$

For every $p = 1, \dots, L$, let $\varepsilon^{(p)} = (1, \dots, 1, 2, \dots, 2)$ where the number of 1's in $\varepsilon^{(p)}$ is exactly p . Properties of the moment measure of Poisson processes (see (Daley and Vere-Jones, 2003) or (Kingman, 1993) in a more simplified framework) lead to

$$\begin{aligned} A_{\varepsilon^{(p)}} &= \mathbb{E} \left[\int_{([a, b]^{(1)})^p ([a, b]^{(2)})^{L-p}} c(x_1, \dots, x_L) c(y_1, \dots, y_L) \prod_{l=1}^L dN_l(x_l) dN_l(y_l) \right] \\ &= \prod_{l=1}^p \lambda_l \prod_{j=p+1}^L \lambda_j^2 \int_{[a, b]^p} \left(\int_{[a, b]^{2(L-p)}} c(t_1, \dots, t_p, x_{p+1}, \dots, x_L) \right. \\ &\quad \left. c(t_1, \dots, t_p, y_{p+1}, \dots, y_L) \prod_{k=p+1}^L dx_k dy_k \right) dt_1 \dots dt_p. \end{aligned} \quad (10)$$

For fixed (t_1, \dots, t_p) one can apply Fubini Theorem to the inner integral which leads to:

$$\begin{aligned} A_{\varepsilon^{(p)}} &= \prod_{l=1}^p \lambda_l \prod_{j=p+1}^L \lambda_j^2 \int_{[a, b]^p} \left(\int_{[a, b]^{2(L-p)}} c(t_1, \dots, t_p, t_{p+1}, \dots, t_J) dt_{p+1} \dots dt_L \right)^2 dt_1 \dots dt_p. \\ &= \prod_{l=1}^p \lambda_l \prod_{j=p+1}^L \lambda_j^2 I(L, L-p). \end{aligned}$$

by definition of $I(L, L-p)$.

For more general vectors ε in $\{1, 2\}^L$, let us note p the occurrence count of 1 in the vector ε and I_{ε} (respectively J_{ε}) the set of indices of the coordinates of ε equal to 1 (respectively 2). Then, using the symmetry of the coincidence function c , one can easily deduce from the computation of $A_{\varepsilon^{(p)}}$ that

$$A_{\varepsilon} = \prod_{i \in I_{\varepsilon}} \lambda_i \prod_{j \in J_{\varepsilon}} \lambda_j^2 I(L, L-p). \quad (11)$$

From (9) and (11), one deduces

$$\mathbb{E}[X_{\mathcal{L}}^2] = \sum_{p=0}^L \left(\sum_{\substack{\mathcal{J} \subseteq \mathcal{L} \\ \#\mathcal{J}=p}} \prod_{j \in \mathcal{J}} \lambda_j \prod_{l \notin \mathcal{J}} \lambda_l^2 \right) I(L, L-p).$$

Note that $I(L, L) = I(L, 0)^2$ by definition, so the case $p = 0$ in the sum corresponds to

$$\prod_{l \in \mathcal{L}} \lambda_l^2 I(L, L) = \prod_{l \in \mathcal{L}} \lambda_l^2 I(L, 0)^2 = \mathbb{E}[X_{\mathcal{L}}]^2.$$

Moreover, the case $p = L$ in the sum corresponds to $\prod_{l \in \mathcal{L}} \lambda_l I(L, 0) = \mathbb{E}[X_{\mathcal{L}}]$. So, we have

$$\mathbb{E}[X_{\mathcal{L}}^2] = \mathbb{E}[X_{\mathcal{L}}]^2 + \mathbb{E}[X_{\mathcal{L}}] + \sum_{p=1}^{L-1} \left(\sum_{\substack{\mathcal{J} \subseteq \mathcal{L} \\ \#\mathcal{J}=p}} \prod_{j \in \mathcal{J}} \lambda_j \prod_{l \notin \mathcal{J}} \lambda_l^2 \right) I(L, L-p),$$

and (6) clearly follows by defining the variable $k = L - p$. □

Theorem 3.1 is a direct consequence of Theorem 8.1 since the function $c_{\delta} : [a, b]^L \rightarrow \{0, 1\}$ defined by

$$c_{\delta}(x_1, \dots, x_n) = \mathbf{1}_{\left| \max_{i \in \{1, \dots, L\}} x_i - \min_{i \in \{1, \dots, L\}} x_i \right| \leq \delta}, \quad 0 < \delta < \frac{b-a}{2} \quad (12)$$

satisfies Definition 8.1.

8.2 Proof of Theorem 3.2

Theorem 8.2. *Under Notations and Assumptions of Theorem 8.1, the two following affirmations are valid:*

- *The following convergence of distribution holds:*

$$\sqrt{M}(\bar{m}_{\mathcal{L}} - \hat{m}_{0, \mathcal{L}}) \xrightarrow[M \rightarrow \infty]{\mathcal{D}} \mathcal{N}(0, \sigma^2),$$

where

$$\sigma^2 = \text{Var}(X_{\mathcal{L}}) - (b-a)^{-1} \mathbb{E}[X_{\mathcal{L}}]^2 \left(\sum_{l \in \mathcal{L}} \lambda_l^{-1} \right).$$

- *Moreover, σ^2 can be estimated by*

$$\hat{\sigma}^2 = \hat{v}(X_{\mathcal{L}}) - (b-a)^{-1} I(L, L) \prod_{l \in \mathcal{L}} \hat{\lambda}_l^2 \left(\sum_{k \in \mathcal{L}} \hat{\lambda}_k^{-1} \right),$$

where

$$\hat{v}(X_{\mathcal{L}}) = \hat{m}_{0, \mathcal{L}} + \sum_{k=1}^{L-1} \left(\sum_{\substack{\mathcal{J} \subseteq \mathcal{L} \\ \#\mathcal{J}=k}} \prod_{j \in \mathcal{J}} \hat{\lambda}_j^2 \prod_{l \notin \mathcal{J}} \hat{\lambda}_l \right) I(L, k),$$

and

$$\sqrt{M} \frac{(\bar{m}_{\mathcal{L}} - \hat{m}_{0, \mathcal{L}})}{\sqrt{\hat{\sigma}^2}} \xrightarrow{\mathcal{D}} \mathcal{N}(0, 1).$$

Proof. For sake of simplicity, the result is proven in the simpler case where $\mathcal{L} = \{1, \dots, L\}$, the generalization being pretty clear. An application of the Central Limit Theorem leads to:

$$\frac{1}{\sqrt{M}} \sum_{k=1}^M \left[\begin{pmatrix} X_{\mathcal{L}}^{(k)} \\ N_1^{(k)}([a, b]) \\ \vdots \\ N_L^{(k)}([a, b]) \end{pmatrix} - \begin{pmatrix} \mathbb{E}[X_{\mathcal{L}}] \\ \lambda_1(b-a) \\ \vdots \\ \lambda_L(b-a) \end{pmatrix} \right] \xrightarrow{\mathcal{D}} \mathcal{N}_{L+1}(\mathbf{0}, \Gamma),$$

where $\mathcal{N}_{L+1}(\mathbf{0}, \Gamma)$ is the multivariate Gaussian distribution with $L+1$ -dimensional mean vector $\mathbf{0}$ and covariance matrix Γ defined by:

$$\Gamma = \begin{pmatrix} \text{Var}(X_{\mathcal{L}}) & \mathbb{E}[X_{\mathcal{L}}] & \cdots & \mathbb{E}[X_{\mathcal{L}}] \\ \mathbb{E}[X_{\mathcal{L}}] & \lambda_1(b-a) & 0 & 0 \\ \vdots & 0 & \ddots & 0 \\ \mathbb{E}[X_{\mathcal{L}}] & 0 & 0 & \lambda_L(b-a) \end{pmatrix}$$

The matrix is obtained using the fact that the processes N_l , $l \in \mathcal{L}$ are independent and from the following computation for all j_0 in \mathcal{L} ,

$$\begin{aligned} \mathbb{E}[X_{\mathcal{L}} N_{j_0}([a, b])] &= \mathbb{E} \left[\int_{[a, b]^{L+1}} c(x_1, \dots, x_L) dN_1(x_1) \dots dN_L(x_L) dN_{j_0}(y) \right] \\ &= \mathbb{E} \left[\int_{[a, b]^{L-1}} \left(\int_{[a, b]^{(2)}} c(x_1, \dots, x_L) dN_{j_0}(x_{j_0}) dN_{j_0}(y) \right) \prod_{l \in \mathcal{L}, l \neq j_0} dN_j(x_j) \right] \\ &\quad + \mathbb{E} \left[\int_{[a, b]^{L-1}} \left(\int_{[a, b]^{(1)}} c(x_1, \dots, x_L) dN_{j_0}(x_{j_0}) dN_{j_0}(y) \right) \prod_{l \in \mathcal{L}, l \neq j_0} dN_j(x_j) \right] \\ &= \lambda_{j_0} \left(\prod_{l \in \mathcal{L}} \lambda_l \right) \int_{[a, b]} \left(\int_{[a, b]^L} c(x_1, \dots, x_L) dx_1 \dots dx_L \right) dy + \left(\prod_{l \in \mathcal{L}} \lambda_l \right) I(L, 0) \\ &\quad \text{(using the same arguments as for (10))} \\ &= \lambda_{j_0}(b-a) \left(\prod_{l \in \mathcal{L}} \lambda_l \right) I(L, 0) + \left(\prod_{l \in \mathcal{L}} \lambda_l \right) I(L, 0) \\ &= \mathbb{E}[N_{j_0}([a, b])] \mathbb{E}[X_{\mathcal{L}}] + \mathbb{E}[X_{\mathcal{L}}], \end{aligned}$$

where $[a, b]^{(2)}$ and $[a, b]^{(1)}$ are defined by (8) in the previous proof. Define

$$g : (x, u_1, \dots, u_L) \mapsto x - (b-a)^{-L} I(L, 0) \prod_{l=1}^L u_l,$$

and remark that:

$$\begin{cases} g \left(\frac{1}{M} \sum_{k=1}^M X_{\mathcal{L}}^{(k)}, \frac{1}{M} \sum_{k=1}^M N_1^{(k)}([a, b]), \dots, \frac{1}{M} \sum_{k=1}^M N_L^{(k)}([a, b]) \right) = \bar{m}_{\mathcal{L}} - \hat{m}_{0, \mathcal{L}}, \\ g(\mathbb{E}[X_{\mathcal{L}}], \lambda_1(b-a), \dots, \lambda_L(b-a)) = 0 \quad \text{(thanks to Theorem 8.1)}. \end{cases}$$

So we have

$$\begin{aligned} \sqrt{M}(\bar{m}_{\mathcal{L}} - \hat{m}_{0, \mathcal{L}}) &= \sqrt{M} \left[g \left(\frac{1}{M} \sum_{k=1}^M X_{\mathcal{L}}^{(k)}, \frac{1}{M} \sum_{k=1}^M N_1^{(k)}([a, b]), \dots, \frac{1}{M} \sum_{k=1}^M N_L^{(k)}([a, b]) \right) \right. \\ &\quad \left. - g(\mathbb{E}[X_{\mathcal{L}}], \lambda_1(b-a), \dots, \lambda_L(b-a)) \right]. \end{aligned}$$

And the delta method (Casella and Berger, 2002) gives the following convergence of distribution,

$$\sqrt{M}(\bar{m}_{\mathcal{L}} - \hat{m}_{0,\mathcal{L}}) \xrightarrow{\mathcal{D}} \mathcal{N}(0, {}^tD\Gamma D),$$

where D is the gradient of the function g at the point $(\mathbb{E}[X_{\mathcal{L}}], \lambda_1(b-a), \dots, \lambda_L(b-a))$ i.e.

$$D = \begin{pmatrix} 1 \\ -\lambda_1^{-1} \mathbb{E}[X_{\mathcal{L}}] (b-a)^{-1} \\ \vdots \\ -\lambda_L^{-1} \mathbb{E}[X_{\mathcal{L}}] (b-a)^{-1} \end{pmatrix}.$$

So,

$$\begin{aligned} {}^tD\Gamma D &= {}^tD \begin{pmatrix} \text{Var}(X_{\mathcal{L}}) - (b-a)^{-1} \mathbb{E}[X_{\mathcal{L}}]^2 (\sum_{l \in \mathcal{L}} \lambda_l^{-1}) \\ \mathbb{E}[X_{\mathcal{L}}] - \mathbb{E}[X_{\mathcal{L}}] \\ \vdots \\ \mathbb{E}[X_{\mathcal{L}}] - \mathbb{E}[X_{\mathcal{L}}] \end{pmatrix} \\ &= \text{Var}(X_{\mathcal{L}}) - (b-a)^{-1} \mathbb{E}[X_{\mathcal{L}}]^2 \left(\sum_{l \in \mathcal{L}} \lambda_l^{-1} \right), \end{aligned}$$

which proves the first part of the Theorem 8.2.

To get the second part, it suffices to apply Slutsky lemma (Casella and Berger, 2002) since the $\hat{\lambda}_l$'s are consistent. \square

Once again, Theorem 3.2 is a direct consequence of Theorem 8.2 since the function $c_{\delta} : [a, b]^L \rightarrow \{0, 1\}$ defined by (12) satisfies Definition 8.1.

8.3 Proof of Proposition 3.1

Here we compute

$$I(L, k) = \int_{[a, b]^{L-k}} \left(\int_{[a, b]^k} \mathbf{1}_{|\max(\vee x_i, \vee y_i) - \min(\wedge x_i, \wedge y_i)| \leq \delta} dx_1 \dots dx_k \right)^2 dy_1 \dots dy_{L-k}$$

where $\wedge x_i = \min\{x_i, i \in \{1, \dots, k\}\}$, $\vee x_i = \max\{x_i, i \in \{1, \dots, k\}\}$ and respectively for $\wedge y_i$ and $\vee y_i$. Let us fix some (y_1, \dots, y_{L-k}) in $[a, b]^{L-k}$ and compute the inner integral

$$\Sigma(y_1, \dots, y_{L-k}) = \int_{[a, b]^k} \mathbf{1}_{|\max(\vee x_i, \vee y_i) - \min(\wedge x_i, \wedge y_i)| \leq \delta} dx_1 \dots dx_k.$$

In order to do that let us decompose the integral with respect to the following conditions on (x_1, \dots, x_k) :

1. if $\wedge x_i > \wedge y_i$ and $\vee x_i > \vee y_i$, denote the integral A ;
2. if $\wedge x_i < \wedge y_i$ and $\vee x_i < \vee y_i$, denote the integral B ;
3. if $\wedge x_i > \wedge y_i$ and $\vee x_i < \vee y_i$, denote the integral C ;
4. if $\wedge x_i < \wedge y_i$ and $\vee x_i > \vee y_i$, denote the integral D .

Since we have partitioned $[a, b]^k$ up to a null measure set, we have $\Sigma(y_1, \dots, y_{L-k}) = A + B + C + D$. Let us show the following equations for all $k = 2, \dots, L-1$,

$$A = \mathbf{1}_{|\vee y_i - \wedge y_i| \leq \delta} \left[(\min(\delta, b - \wedge y_i))^k - (\vee y_i - \wedge y_i)^k \right], \quad (13)$$

$$B = \mathbf{1}_{|\vee y_i - \wedge y_i| \leq \delta} \left[(\min(\delta, \vee y_i - a))^k - (\vee y_i - \wedge y_i)^k \right], \quad (14)$$

$$C = \mathbf{1}_{|\vee y_i - \wedge y_i| \leq \delta} (\vee y_i - \wedge y_i)^k, \quad (15)$$

$$\begin{aligned} D = & \mathbf{1}_{|\vee y_i - \wedge y_i| \leq \delta} \left[(\vee y_i - \wedge y_i)^k - (\min(\delta, \vee y_i - a))^k \right. \\ & \left. + k(\min(\wedge y_i, b - \delta) - \max(\vee y_i - \delta, a)) \delta^{k-1} + (\max(\delta, b - \wedge y_i))^k - (b - \wedge y_i)^k \right] \end{aligned} \quad (16)$$

and

$$\Sigma(y_1, \dots, y_{L-k}) = \mathbf{1}_{|\vee y_i - \wedge y_i| \leq \delta} [(k+1)\delta^k + k(\min(\wedge y_i, b - \delta) - \max(\vee y_i, a + \delta))\delta^{k-1}]. \quad (17)$$

Let us fix some k in $\{2, \dots, L-1\}$.

Proof of (13) To compute A , it is sufficient to consider the case when $x_1 = \vee x_i$, provided a multiplication by k , hence

$$\begin{aligned} A &= k \int_{x_1 = \vee y_i}^b \left(\int_{[\wedge y_i, x_1]^{k-1}} \mathbf{1}_{|x_1 - \wedge y_i| \leq \delta} dx_2 \dots dx_k \right) dx_1 \\ &= k \mathbf{1}_{|\vee y_i - \wedge y_i| \leq \delta} \int_{x_1 = \vee y_i}^{\min(\wedge y_i + \delta, b)} \left(\int_{[\wedge y_i, x_1]^{k-1}} 1 dx_2 \dots dx_k \right) dx_1 \\ &= k \mathbf{1}_{|\vee y_i - \wedge y_i| \leq \delta} \int_{x_1 = \vee y_i}^{\min(\wedge y_i + \delta, b)} (x_1 - \wedge y_i)^{k-1} dx_1 \\ &= \mathbf{1}_{|\vee y_i - \wedge y_i| \leq \delta} \left[(\min(\wedge y_i + \delta, b) - \wedge y_i)^k - (\vee y_i - \wedge y_i)^k \right] \\ &= \mathbf{1}_{|\vee y_i - \wedge y_i| \leq \delta} \left[(\min(\delta, b - \wedge y_i))^k - (\vee y_i - \wedge y_i)^k \right]. \end{aligned}$$

Proof of (14) To calculate B , we use the same idea and consider the case when $x_1 = \wedge x_i$, leading to

$$\begin{aligned} B &= k \int_{x_1 = \max(\vee y_i - \delta, a)}^{\wedge y_i} (\vee y_i - x_1)^{k-1} dx_1 \\ &= \mathbf{1}_{|\vee y_i - \wedge y_i| \leq \delta} \left[(\vee y_i - \max(\vee y_i - \delta, a))^k - (\vee y_i - \wedge y_i)^k \right] \\ &= \mathbf{1}_{|\vee y_i - \wedge y_i| \leq \delta} \left[(\min(\delta, \vee y_i - a))^k - (\vee y_i - \wedge y_i)^k \right]. \end{aligned}$$

Proof of (15) This case is pretty clear.

$$C = \int_{[\wedge y_i, \vee y_i]^k} \mathbf{1}_{|\vee y_i - \wedge y_i| \leq \delta} dx_1 \dots dx_k = \mathbf{1}_{|\vee y_i - \wedge y_i| \leq \delta} (\vee y_i - \wedge y_i)^k$$

Proof of (16) To calculate D , it is sufficient to consider the case when $x_1 = \wedge x_i$ and $x_2 = \vee x_i$, provided a multiplication by $k(k-1)$, hence

$$\begin{aligned} D &= k(k-1) \int_{x_1 = a}^{\wedge y_i} \int_{x_2 = \vee y_i}^b \left(\int_{x_1}^{x_2} \mathbf{1}_{|x_2 - x_1| \leq \delta} dx_3 \dots dx_k \right) dx_2 dx_1 \\ &= k(k-1) \mathbf{1}_{|\vee y_i - \wedge y_i| \leq \delta} \int_{x_1 = \max(\vee y_i - \delta, a)}^{\wedge y_i} \int_{x_2 = \vee y_i}^{\min(x_1 + \delta, b)} (x_2 - x_1)^{k-2} dx_2 dx_1 \\ &= k \mathbf{1}_{|\vee y_i - \wedge y_i| \leq \delta} \int_{x_1 = \max(\vee y_i - \delta, a)}^{\wedge y_i} (\min(x_1 + \delta, b) - x_1)^{k-1} - (\vee y_i - x_1)^{k-1} dx_1 \\ &= \mathbf{1}_{|\vee y_i - \wedge y_i| \leq \delta} \left[(\vee y_i - \wedge y_i)^k - (\vee y_i - \max(\vee y_i - \delta, a))^k \right. \\ &\quad \left. + k(\min(\wedge y_i, b - \delta) - \max(\vee y_i - \delta, a))\delta^{k-1} + (b - \min(\wedge y_i, b - \delta))^k - (b - \wedge y_i)^k \right] \\ &= \mathbf{1}_{|\vee y_i - \wedge y_i| \leq \delta} \left[(\vee y_i - \wedge y_i)^k - (\min(\delta, \vee y_i - a))^k \right. \\ &\quad \left. + k(\min(\wedge y_i, b - \delta) - \max(\vee y_i - \delta, a))\delta^{k-1} + (\max(\delta, b - \wedge y_i))^k - (b - \wedge y_i)^k \right]. \end{aligned}$$

Proof of (17) Remark that

$$(\min(\delta, b - \wedge y_i))^k + (\max(\delta, b - \wedge y_i))^k = \delta^k + (b - \wedge y_i)^k \quad (18)$$

and

$$\max(\vee y_i - \delta, a) = \max(\vee y_i, a + \delta) - \delta. \quad (19)$$

Gathering (13), (14), (15), (16), (18) and (19) gives (17). Hence, Equation (17) holds for every k in $\{2, \dots, L-1\}$.

Moreover, if $k = 0$, then $\Sigma(y_1, \dots, y_{L-k}) = \mathbf{1}_{|\vee y_i - \wedge y_i| \leq \delta}$ and, if $k = 1$, then $\Sigma(y_1, \dots, y_{L-k}) = \mathbf{1}_{|\vee y_i - \wedge y_i| \leq \delta} [\min(\wedge y_i + \delta, b) - \max(\vee y_i - \delta, a)]$. To summarize, Equation (17) holds for every k in $\{0, \dots, L-1\}$.

It remains to compute

$$I(L, k) = \int_{[a, b]^{L-k}} \Sigma(y_1, \dots, y_{L-k})^2 dy_1 \dots dy_{L-k}.$$

In order to do that, let us decompose the integral with respect to the following conditions on (y_1, \dots, y_{L-k}) :

1. $\vee y_i < a + \delta$. In this case, $\Sigma = \delta^{k-1} [\delta + k(\wedge y_i - a)]$, and denote the integral Y .
2. $\wedge y_i > b - \delta$. In this case, $\Sigma = \delta^{k-1} [\delta + k(b - \vee y_i)]$, and denote the integral Z .
3. $\vee y_i > a + \delta$ and $\wedge y_i < b - \delta$. In this case, $\Sigma = \mathbf{1}_{|\vee y_i - \wedge y_i| \leq \delta} \delta^{k-1} [(k+1)\delta - k(\vee y_i - \wedge y_i)]$, and denote the integral W .

These three cases are distinct because $\delta < (b-a)/2$, so we have partitioned $[a, b]^{L-k}$ up to a null measure set and $I(L, k) = Y + Z + W$. Let us show the following equations for all $k = 0, \dots, L-2$,

$$Y = Z = C(L, k) \delta^{L+k}, \quad (20)$$

$$W = f(L, k) (b-a) \delta^{L+k-1} - [f(L, k) + g(L, k)] \delta^{L+k}, \quad (21)$$

where

$$C(L, k) = (L-k) \frac{(k+1)^{L-k+2}}{k^{L-k}} \int_0^{\frac{k}{k+1}} t^{L-k-1} (1-t)^2 dt, \quad (22)$$

$$f(L, k) = (L-k)(k+1)^2 - 2(L-k-1)k(k+1) + \frac{(L-k)(L-k-1)}{(L-k+1)} k^2$$

and

$$g(L, k) = (k+1)^2 - 2 \frac{(L-k-1)k(k+1)}{(L-k+1)} + \frac{(L-k)(L-k-1)}{(L-k+1)(L-k+2)} k^2.$$

Let us fix some k in $\{0, \dots, L-2\}$.

Proof of (20) To compute Y , it is sufficient to consider the case when $y_1 = \wedge y_i$, provided a multiplication by $(L-k)$, hence

$$\begin{aligned} Y &= \int_{\vee y_i \leq a+\delta} \Sigma(y_1, \dots, y_{L-k})^2 dy_1 \dots dy_{L-k} \\ &= (L-k) \delta^{2k-2} \int_{y_1=a}^{a+\delta} \left(\int_{[y_1, a+\delta]^{L-k-1}} [\delta + k(y_1 - a)]^2 dy_2 \dots dy_{L-k} \right) dy_1 \\ &= (L-k) \delta^{2k-2} \int_{y_1=a}^{a+\delta} (a+\delta - y_1)^{L-k-1} [\delta + k(y_1 - a)]^2 dy_1. \end{aligned}$$

Defining the variable $u = a + \delta - y_1$ leads to

$$\begin{aligned} Y &= (L-k) \delta^{2k-2} \int_0^\delta u^{L-k-1} [\delta + k(\delta - u)]^2 du \\ &= (L-k) \delta^{2k-2} \int_0^\delta u^{L-k-1} [(k+1)\delta - ku]^2 du, \end{aligned}$$

and by defining the variable $t = \frac{ku}{(k+1)\delta}$ we have

$$\begin{aligned} Y &= (L-k) \delta^{2k-2} \int_0^{\frac{k}{k+1}} \left(\frac{(k+1)\delta t}{k} \right)^{L-k-1} (k+1)^2 \delta^2 (1-t)^2 \frac{(k+1)\delta}{k} dt \\ &= (L-k) \delta^{L+k} \frac{(k+1)^{L-k+2}}{k^{L-k}} \int_0^{\frac{k}{k+1}} t^{L-k-1} (1-t)^2 dt. \end{aligned}$$

The computation of Z can be done in the same way by inverting the roles of a and b on the one hand and the roles of $\wedge y_i$ and $\vee y_i$ on the other hand. This leads to $Z = Y$ and Equation (20).

Proof of (21) To compute W , it is sufficient to consider the case when $y_1 = \wedge y_i$ and $y_2 = \vee y_i$, provided a multiplication by $(L-k)(L-k-1)$, hence

$$\begin{aligned} W &= (L-k)(L-k-1) \delta^{2k-2} \\ &\quad \int_{y_1=a}^{b-\delta} \int_{y_2=\max(y_1, a+\delta)}^b \left(\int \mathbf{1}_{|y_2-y_1| \leq \delta} [(k+1)\delta - k(y_2 - y_1)]^2 dy_3 \dots dy_{L-k} \right) dy_2 dy_1 \\ &= (L-k)(L-k-1) \delta^{2k-2} \\ &\quad \int_{y_1=a}^{b-\delta} \int_{y_2=\max(y_1, a+\delta)}^{y_1+\delta} \left((y_2 - y_1)^{L-k-2} \left[(k+1)^2 \delta^2 - 2k(k+1)\delta(y_2 - y_1) \right. \right. \\ &\quad \left. \left. + k^2 (y_2 - y_1)^2 \right] \right) dy_2 dy_1, \end{aligned}$$

which leads to

$$\begin{aligned} W &= \int_a^{b-\delta} \left\{ (L-k) \delta^{2k-2} (k+1)^2 \delta^2 \left[\delta^{L-k-1} - (\max(y_1, a+\delta) - y_1)^{L-k-1} \right] \right\} \\ &\quad - \left\{ 2(L-k-1) \delta^{2k-2} k(k+1) \delta \left[\delta^{L-k} - (\max(y_1, a+\delta) - y_1)^{L-k} \right] \right\} \\ &\quad + \left\{ \frac{(L-k)(L-k-1)}{(L-k+1)} \delta^{2k-2} k^2 \left[\delta^{L-k+1} - (\max(y_1, a+\delta) - y_1)^{L-k+1} \right] \right\} dy_1 \\ &= W_1 + W_2, \end{aligned}$$

where W_1 (resp. W_2) denotes the integral between a and $a+\delta$ (resp. between $a+\delta$ and $b-\delta$). Let us denote

$$f(L, k) = (L-k)(k+1)^2 - 2(L-k-1)k(k+1) + \frac{(L-k)(L-k-1)}{(L-k+1)} k^2. \quad (23)$$

Then, on the one hand

$$\begin{aligned} W_1 &= \delta^{2k-2} \left[\int_a^{a+\delta} f(L, k) \delta^{L-k+1} dy_1 \right. \\ &\quad - (L-k)(k+1)^2 \delta^2 \int_a^{a+\delta} (a+\delta - y_1)^{L-k-1} dy_1 \\ &\quad + 2(L-k-1)k(k+1) \delta \int_a^{a+\delta} (a+\delta - y_1)^{L-k} dy_1 \\ &\quad \left. - \frac{(L-k)(L-k-1)}{(L-k+1)} k^2 \int_a^{a+\delta} (a+\delta - y_1)^{L-k+1} dy_1 \right] \\ &= f(L, k) \delta^{L+k} - g(L, k) \delta^{L+k}, \end{aligned}$$

with

$$g(L, k) = (k+1)^2 - 2 \frac{(L-k-1)k(k+1)}{(L-k+1)} + \frac{(L-k)(L-k-1)}{(L-k+1)(L-k+2)} k^2. \quad (24)$$

On the other hand,

$$\begin{aligned} W_2 &= \delta^{2k-2} \int_{a+\delta}^{b-\delta} \left[(L-k)(k+1)^2 - 2(L-k-1)k(k+1) \right. \\ &\quad \left. + \frac{(L-k)(L-k-1)}{(L-k+1)} k^2 \right] \delta^{L-k+1} dy_1 \\ &= (b-a-2\delta) f(L, k) \delta^{L+k-1} \\ &= f(L, k) (b-a) \delta^{L+k-1} - 2f(L, k) \delta^{L+k} \end{aligned}$$

where $f(L, k)$ is defined by (23). Then, (21) clearly follows from $W = W_1 + W_2$.

Moreover, if $k = L - 1$, then Equations (20) and (21) are still valid. To summarize, Equations (20) and (21) hold true for every k in $\{0, \dots, L-1\}$.

Gathering (20) and (21) yields

$$I(L, k) = f(L, k) (b-a) \delta^{L+k-1} - [f(L, k) + g(L, k) - 2C(L, k)] \delta^{L+k},$$

for every k in $\{0, \dots, L-1\}$.

To conclude, the integral involved in (22) can be computed with respect to k and L in the following way,

$$\int_0^{\frac{k}{k+1}} t^{L-k-1} (1-t)^2 dt = \left(\frac{k}{k+1} \right)^{L-k} \left[\frac{1}{L-k} - \frac{2k}{(k+1)(L-k+1)} + \frac{k^2}{(k+1)^2(L-k+2)} \right].$$

Moreover, in the result stated in Proposition 3.1 we just used the software Mathematica in order to simplify the expressions. These simplifications lead to

$$f(L, k) = \frac{k(k+1) + L(L+1)}{L-k+1}$$

and

$$h(L, k) := f(L, k) + g(L, k) - 2C(L, k) = \frac{-k^3 + k^2(2+L) + k(5+2L-L^2) + L^3 + 2L^2 - L - 2}{(L-k+2)(L-k+1)}.$$

References

- Abeles, M. (1982), ‘Quantification, smoothing, and confidence limits for single-units’ histograms’, *Journal of Neuroscience Methods* **5**(4), 317–325.
- Aertsen, A. M. H. J., Gerstein, G. L., Habib, M. K. and Palm, G. (1989), ‘Dynamics of Neuronal Firing Correlation: Modulation of “Effective Connectivity”’, *Journal of Neurophysiology* **61**, 900–917.
- Albert, M., Bouret, Y., Fromont, M. and Reynaud-Bouret, P. (2014), ‘Bootstrap and permutation tests of independence for point processes’, prepublication on HAL .
- Archer, E. W., Park, I. M. and Pillow, J. W. (2013), Bayesian entropy estimation for binary spike train data using parametric prior knowledge, in ‘Advances in Neural Information Processing Systems’, pp. 1700–1708.
- Barlow, H. B. (1972), ‘Single Units and Sensation: A Neuron Doctrine for Perceptual Psychology?’, *Perception* **1**, 371–394.
- Benjamini, Y. and Hochberg, Y. (1995), ‘Controlling the false discovery rate: a practical and powerful approach to multiple testing’, *Journal of the Royal Statistical Society. Series B. Methodological* **57**(1), 289–300.
- Borgelt, C. and Muiño, D. (2013), Finding Frequent Patterns in Parallel Point Processes, Advances in Intelligent Data Analysis XII, 116–126.
- Brown, E. N., Kass, R. E. and Mitra, P. P. (2004), ‘Multiple neural spike train data analysis: state-of-the-art and future challenges’, *Nature Neuroscience* **26**(7), 456–461.
- Casella, G. and Berger, R. (2002), *Statistical Inference*, Duxbury.
- Chornoboy, E., Schramm, L. and Karr, A. (1988), ‘Maximum likelihood identification of neural point process systems’, *Biological Cybernetics* **59**(4-5), 265–275.
- Daley, D. J. and Vere-Jones, D. (2003), *An introduction to the theory of point processes. Vol. I, Probability and its Applications* (New York), second edn, Springer-Verlag, New York. Elementary theory and methods.
- Gerstein, G. L., Aertsen, A. M. et al. (1985), ‘Representation of cooperative firing activity among simultaneously recorded neurons’, *Journal of Neurophysiology* **54**(6), 1513–1528.
- Gerstein, G. L. and Perkel, D. H. (1969), ‘Simultaneously Recorded Trains of Action Potentials: Analysis and Functional Interpretation’, *Science* **164**(3881), 828–830.
- Grammont, F. and Riehle, A. (2003), ‘Spike synchronization and firing rate in a population of motor cortical neurons in relation to movement direction and reaction time.’, *Biological Cybernetics* **88**(5), 360–373.
- Grün, S. (1996), Unitary joint events in multiple neuron spiking activity: detection, significance, and interpretation, PhD thesis.
- Grün, S. (2009), Data-driven significance estimation for precise spike correlation, *Journal of Neurophysiology* **101**.
- Grün, S., Diesmann, M. and Aertsen, A. (2002), ‘Unitary Events in Multiple Single-Neuron Spiking Activity: I. Detection and Significance.’, *Neural Computation* **14**(1), 43–80.
- Grün, S., Diesmann, M., Grammont, F., Riehle, A. and Aertsen, A. (1999), ‘Detecting unitary events without discretization of time’, *Journal of neuroscience methods* **94**(1), 67–79.
- Harrison, M. and Geman, S. (2009), A rate and history-preserving resampling algorithm for neural spike trains, *Neural Computation* **21**, 1244–1258.
- Hebb, D. O. (1949), *The Organization of Behavior: A Neuropsychological Theory*, Wiley, New York.

- Kingman, J. F. C. (1993), *Poisson processes*, Vol. 3 of *Oxford Studies in Probability*, The Clarendon Press Oxford University Press, New York. Oxford Science Publications.
- Krumin, M., Reutsky, I. and Shoham, S. (2010), ‘Correlation-based analysis and generation of multiple spike trains using Hawkes models with an exogenous input’, *Frontiers in computational neuroscience* **4**.
- Lehmann, E. and Romano, J. P. (2005), *Testing Statistical Hypotheses*, 3rd edn, Springer-Verlag New York Inc.
- Lewis, P. A. W. and Shedler, G. S. (1979), ‘Simulation of nonhomogeneous Poisson processes by thinning’, *Naval Research Logistics Quarterly* **26**(3), 403–413.
- Louis, S., Gerstein, G., Grün, S. and Diesmann, M. (2010), Surrogate spike train generation through dithering in operational time, *Frontiers in computational neuroscience* **4**.
- Louis, S., Borgelt, C., and Grün, S. (2010), Generation and selection of surrogate methods for correlation analysis, in S. Grün and S. Rotter, eds, ‘Analysis of Parallel Spike Trains’, Vol. 7 of *Springer Series in Computational Neuroscience*, Springer US, pp. 359–382.
- Muñoz, D. and Borgelt, C. (2014), Frequent item set mining for sequential data: Synchrony in neuronal spike trains, *Intelligent Data Analysis*, **18**, 997–1012
- Ogata, Y. (1981), ‘On Lewis simulation method for point processes’, *IEEE Transactions on Information Theory* **27**(1), 23–30.
- Palm, G. (1990), ‘Cell assemblies as a guideline for brain research’, *Concepts in Neuroscience* **1**(1), 133–147.
- Perkel, D. H., Gerstein, G. L. and Moore, G. P. (1967), ‘Neuronal Spike Trains and Stochastic Point Processes: II. Simultaneous Spike Trains’, *Biophysical Journal* **7**(4), 419–440.
- Pernice, V., Staude, B., Cardanobile, S. and Rotter, S. (2011), ‘How structure determines correlations in neuronal networks’, *Public Library of Science: Computational Biology* **7**(5), e1002059.
- Pernice, V., Staude, B., Cardanobile, S. and Rotter, S. (2012), ‘Recurrent interactions in spiking networks with arbitrary topology’, *Physical Review E* **85**(3), 031916.
- Pipa, G., Diesmann, M. and Grün, S. (2003), ‘Significance of joint-spike events based on trial-shuffling by efficient combinatorial methods’, *Complexity* **8**(4), 79–86.
- Pipa, G. and Grün, S. (2003), ‘Non-parametric significance estimation of joint-spike events by shuffling and resampling’, *Neurocomputing* **52**, 31–37.
- Reimer, I. C., Staude, B., Ehm, W. and Rotter, S. (2012), ‘Modeling and analyzing higher-order correlations in non-Poissonian spike trains’, *Journal of neuroscience methods* **208**(1), 18–33.
- Reynaud-Bouret, P., Rivoirard, V., Grammont, F. and Tuleau-Malot, C. (2014), Goodness-of-fit tests and nonparametric adaptive estimation for spike train analysis, *The Journal of Mathematical Neuroscience (JMN)* **4**, 1–41.
- Riehle, A., Grammont, F., Diesmann, M. and Grün, S. (2000), ‘Dynamical changes and temporal precision of synchronized spiking activity in monkey motor cortex during movement preparation’, *Journal of Physiology-Paris* **94**(5), 569–582.
- Riehle, A., Grammont, F. and MacKay, W. A. (2006), ‘Cancellation of a planned movement in monkey motor cortex’, *Neuroreport* **17**(3), 281–285.
- Sakurai, Y. (1999), ‘How do cell assemblies encode information in the brain?’, *Neuroscience & Biobehavioral Reviews* **23**(6), 785–796.
- Shinomoto, S. (2010), Estimating the Firing Rate, in S. Grün and S. Rotter, eds, ‘Analysis of Parallel Spike Trains’, Vol. 7 of *Springer Series in Computational Neuroscience*, Springer US, pp. 21–35.

- Singer, W. (1993), ‘Synchronization of Cortical Activity and its Putative Role in Information Processing and Learning’, *Annual Review of Physiology* **55**, 349–374.
- Stark, E. and Abeles, M. (2009), Unbiased estimation of precise temporal correlations between spike trains, *Journal of neuroscience methods* **179**, 90–100.
- Tuleau-Malot, C., Rouis, A., Grammont, F. and Reynaud-Bouret, P. (2014), ‘Multiple Tests Based on a Gaussian Approximation of the Unitary Events Method with delayed coincidence count’, appearing in *Neural Computation* **26:7**.
- von der Malsburg, C. (1981), The Correlation Theory of Brain Function, Internal Report 81-2, Department of Neurobiology, Max-Planck-Institute for Biophysical Chemistry, Göttingen, Germany.
- Pillow, J. W., Shlens, J., Paninski, L., Sher, A., Litke, A. M., Chichilnisky, E. J., and Simoncelli, E. P. (2008), ‘Spatio-temporal correlations and visual signalling in a complete neuronal population’, *Nature*, 995–999.
- A. Roy , P. N. Steinmetz , S. S. Hsiao , K. O. Johnson and E. Niebur (2007), ‘Synchrony: A Neural Correlate of Somatosensory Attention’, *Journal of Neurophysiology*, **98 (3)** 1645–1661.
- Dong, Y., Mihalas, S., Qiu, F., von der Heydt, R., and Niebur, E. (2008), ‘Synchrony and the binding problem in macaque visual cortex’, *Journal of Vision*, **8(7)** 30.

References